

1 **Characterization of highly ferulate-tolerant *Acinetobacter baylyi* ADP1 isolates**
2 **by a rapid reverse-engineering method**

3 Jin Luo^{1#}, Emily A. McIntyre², Stacy R. Bedore², Ville Santala¹, Ellen L. Neidle², Suvi Santala¹

4 ¹Faculty of Engineering and Natural Sciences, Hervanta campus, Tampere University,

5 Korkeakoulunkatu 8, Tampere, 33720, Finland

6 ²Department of Microbiology, University of Georgia, Athens, GA 30602-2605 USA

7 Running head: Characterization of ferulate-tolerant isolates

8 Keywords: adaptive laboratory evolution; aromatic acids; tolerance; reverse engineering;

9 *Acinetobacter baylyi* ADP1

10 #Address correspondence to Jin Luo: jin.luo@tuni.fi

11 Emily A. McIntyre: emcintyre@uga.edu

12 Stacy R. Bedore: stacybedore@uga.edu

13 Ville Santala: ville.santala@tuni.fi

14 Ellen L. Neidle: eneidle@uga.edu

15 Suvi Santala: suvi.santala@tuni.fi

16 **Abstract**

17 Adaptive laboratory evolution (ALE) is a powerful approach for improving phenotypes of
18 microbial hosts. Evolved strains typically contain numerous mutations that can be revealed by
19 whole-genome sequencing. However, determining the contribution of specific mutations to new
20 phenotypes is typically challenging and laborious. This task is complicated by factors such as the
21 mutation type, the genomic context, and the interplay between different mutations. Here, a novel
22 approach was developed to identify the significance of mutations in strains evolved from
23 *Acinetobacter baylyi* ADP1. This method, termed Rapid Advantageous Mutation ScrEening and
24 Selection (RAMSES), was used to analyze mutants that emerged from stepwise adaptation to, and
25 consumption of, high levels of ferulate, a common lignin-derived aromatic compound. After
26 whole-genome sequence analysis, RAMSES allowed rapid determination of effective mutations
27 and seamless introduction of the beneficial mutations into the chromosomes of new strains with
28 different genetic backgrounds. This simple approach to reverse-engineering exploits the natural
29 competence and high recombination efficiency of ADP1. Mutated DNA, added directly to growing
30 cells, replaces homologous chromosomal regions to generate transformants that will become
31 enriched if there is selective benefit. Thus, advantageous mutations can be rapidly identified. Here,
32 the growth advantage of transformants under selective pressure revealed key mutations in genes
33 related to aromatic transport, including *hcaE*, *hcaK*, and *vanK*, and a gene, *ACIAD0482*, which is
34 associated with lipopolysaccharide synthesis. This study provides insights into enhanced
35 utilization of industrially relevant aromatic substrates and demonstrates the use of *A. baylyi* ADP1
36 as a convenient platform for strain development and evolution studies.

37 **Importance**

38 Microbial conversion of lignin-enriched streams is a promising approach for lignin valorization.
39 However, the lignin-derived aromatic compounds are toxic to cells at relevant concentrations.
40 Although adaptive laboratory evolution (ALE) is a powerful approach to develop more tolerant
41 strains, it is typically laborious to identify the mechanisms underlying phenotypic improvement.
42 We employed *Acinetobacter baylyi* ADP1, an aromatic compound degrading strain that may be
43 useful for biotechnology. The natural competence and high recombination efficiency of this strain
44 can be exploited for critical applications such as the breakdown of lignin and plastics, abundant
45 polymers composed of aromatic subunits. The natural transformability of this bacterium enabled
46 us to develop a novel approach for rapid screening of advantageous mutations from ALE-derived
47 aromatic-tolerant ADP1-derived strains. We clarified the mechanisms and genetic targets for
48 improved tolerance towards common lignin-derived aromatic compounds. This study facilitates
49 metabolic engineering for lignin valorization.

50 **1. Introduction**

51 The importance of adaptive laboratory evolution (ALE) (1, 2) in generating strains with desired
52 traits is evidenced by success in improving the tolerance of production hosts towards stresses
53 caused by non-optimal pH levels (3), high substrate or product concentrations (2, 4, 5), or other
54 growth inhibitors (6, 7). Discovery of the associated genetic change can be accomplished by
55 whole-genome sequencing (1, 2). However, it is challenging to determine the contribution of
56 mutations, alone or in combination, to the evolved phenotype, as ALE typically yields multiple
57 mutations (2). In addition, mutations may occur in poorly characterized genes. Some mutations

58 may be neutral, others important for the evolutionary trajectory but not the final phenotype, and
59 yet others may be deleterious hitchhikers (2).

60 Statistical methods have the potential to predict relevant mutations across a large number of
61 independent ALE experiments (8), but a more profound understanding of the functional relevance
62 of genetic change requires the reconstruction of strains with specific mutations (2). Such
63 reconstruction, also referred to as reverse engineering, can be done by the introduction of selected
64 mutations into reference strains, followed by comparative analyses (5, 7, 9–11). However,
65 significant efforts may be required to synthesize alleles and integrate genetic changes in the
66 appropriate location, especially when multiple mutations are tested. The bacterium used in our
67 experiments, *Acinetobacter baylyi* ADP1 (hereafter ADP1), has unique advantages for
68 determining the combinatorial effects of mutations. Its high efficiency of natural transformation
69 and allelic replacement have long been exploited because linear DNA can be added directly to
70 growing cultures. DNA responsible for a new phenotype is readily identified when it confers a
71 growth advantage (12). As described here, we developed a high throughput method for the
72 simultaneous analysis of multiple ALE-generated mutations.

73 ADP1 is an ideal model organism for biotechnology and synthetic biology (13) that has been used
74 to study bacterial metabolism, engineering, and evolution (14–17). The potential of ADP1 as a
75 production host for the synthesis of both native (18–22) and non-native products (20, 23, 24) has
76 also been demonstrated. In our previous study, we engineered ADP1 for the production of 1-
77 alkenes from ferulate (23), which represents one of the major compounds of alkaline-pretreated
78 lignin (25–27). Engineering aromatic compound catabolism to valorize the lignin fraction of
79 lignocellulose has important industrial potential (28, 29), and ADP1 is among the best bacterial
80 candidates for this purpose (26). However, due to the inhibitory effects of lignin-derived aromatic

81 compounds and the complexity of the associated pathways, natural pathways are not yet optimal
82 for lignin valorization.

83 In this study, ALE was used to increase the tolerance and utilization of aromatic compounds to
84 improve the suitability of ADP1 for these biotechnology applications. Catabolic pathways for
85 aromatic compound degradation via the β -ketoacid pathway in ADP1 and other bacteria have
86 been well characterized (30–32). ALE has been shown to be effective in overcoming problematic
87 aspects of complex regulation, transport, and enzyme specificity for aromatic compound
88 degradation (17, 33). As described in this report, we characterized the phenotypes of different ALE
89 lineages followed by whole-genome sequencing. Our new method, Rapid Advantageous Mutation
90 ScrEening and Selection (RAMSES), facilitated the identification of the relevant mutations and
91 the reverse engineering process. The method relies on simple recreation of mutated chromosomal
92 alleles by transforming growing cells directly with DNA, followed by efficient enrichment of
93 beneficial transformants under suitable selective pressure. Finally, strains with increased tolerance
94 were reconstructed by the new method and characterized. This study provides insights into
95 enhancing the tolerance of production hosts towards lignin-derived aromatics and highlights the
96 utility of ADP1.

97 **2. Results**

98 **2.1. Adaptive laboratory evolution of *A. baylyi* ADP1 for high ferulate tolerance**

99 Two parallel evolutions were previously carried out for ADP1 to improve the growth on ferulate
100 as a sole carbon source (23), designated as G1 and G2 evolution lines here (Figure S1A). Here, we
101 carried out the ALE experiment also for two additional lineages to improve the tolerance towards
102 ferulate, where 0.2% (w/v) casamino acids and 10 mM acetate were supplied along with ferulate,

103 designated as T1 and T2 evolution lines (Figure S1A). Acetate was added as an additional carbon
104 source, as acetate is present in substantial amounts in the commonly used lignin-enriched stream
105 (25, 26). This approach allows finding mutations that are potentially advantageous for both
106 tolerance and utilization of aromatic compounds. To develop highly ferulate-tolerant strains,
107 ferulate concentration was increased step-wise during the evolution experiments (Figure S1B). A
108 starting concentration of 55 mM was applied to the T1 and T2 evolution lines. The cells were daily
109 passaged to fresh media for two months (370-390 generations), with the endpoint ferulate
110 concentration being 135 mM for the T1/T2 evolution line. Individual isolates were obtained from
111 end-point populations. Four isolates, which were named using ASA strain designations, were used
112 for the subsequent studies (Figure S1): ASA500 and ASA501 were from G1 and G2 evolution
113 lines respectively, and ASA502 and ASA503, were both from the T2 evolution line.

114 **2.2. Characterization of the evolved strains**

115 The evolved strains ASA500, ASA501, ASA502, and ASA503 were cultivated at different ferulate
116 concentrations in 96-well plates, and wild-type ADP1, designated as WT ADP1, was used as the
117 control. It was noted that a biphasic growth pattern was observed in some cases when cells were
118 grown on the aromatic substrates (Figure S2). Therefore, to evaluate the tolerance of strains
119 consistently and comprehensively at different conditions, we decided to use the time needed for
120 cells to reach OD 0.8 as an indicator (later $t_{OD\ 0.8}$). This indicator is influenced by both lag phase
121 and growth rate.

122 All the evolved strains exhibited improved tolerance to ferulate, ASA500 had the best $t_{OD\ 0.8}$ value
123 (ASA500 and ASA501 Figure 1B, ASA502 and ASA503 Figure S3). In the presence of 20 mM
124 ferulate, the $t_{OD\ 0.8}$ was 42.5 h for WT ADP1, 12 h for ASA500, and 16 h for ASA501 (Figure 1B).
125 For WT ADP1, a long lag phase accounted for most of $t_{OD\ 0.8}$. When ferulate concentration was

126 increased to 80 mM, the growth of WT ADP1 was completely inhibited while the $t_{OD\ 0.8}$ value was
127 prolonged to 17 h for ASA500, and 33.5 h for ASA501 (Figure 1B). A similar experimental set-
128 up was employed to test the growth of ASA500 and ASA501 on *p*-coumarate and vanillate. *p*-
129 coumarate, ferulate, and vanillate are all catabolized through the protocatechuate branch of the β -
130 ketoadipate pathway. Vanillate is also an intermediate metabolite in the catabolism of ferulate (34)
131 (Figure 1A). Improved tolerance towards *p*-coumarate and vanillate was also observed from the
132 two isolates ASA500 and ASA501 (Figure 1B). Vanillate seemed to be less toxic than ferulate and
133 *p*-coumarate, as indicated by the growth of WT ADP1 on this substrate.

134 Although ASA502 and ASA503 evolved in the presence of 0.2% casamino acids and 10 mM
135 acetate, both showed improved growth in ferulate as the sole carbon source (Figure S3). The two
136 strains were further cultivated in elevated ferulate concentrations while being supplemented with
137 casamino acids and acetate. When the ferulate concentration was increased from 40 mM to 80 mM,
138 there was a 5 h of increase in the $t_{OD\ 0.8}$ for both strains (Figure S4), which was shorter than the
139 greater than 10 h increase observed when ferulate was the sole carbon source (Figure S3). In 40
140 mM ferulate, WT ADP1 showed diauxic growth characteristic of the sequential consumption of
141 carbon sources; the aromatic degradative pathway is known to be repressed in the presence of
142 acetate through catabolite repression (31). Diauxic growth was not observed for ASA502 and
143 ASA503. However, HPLC analysis showed that while acetate and ferulate were consumed
144 sequentially when both substrates were present, the ferulate was rapidly consumed after acetate
145 was depleted (data not shown). Interestingly, an increase of acetate concentration from 10 mM to
146 50 mM improved the tolerance of WT ADP1 towards ferulate (Figure S4).

147 The tolerance towards aromatic acids may also be affected by the pH of media, possibly related to
148 the protonation of the acids. Protonated aromatic acids can passively diffuse across bacterial cell

149 membranes (35). The results in a Supplemental Note demonstrated an improved growth of WT
150 ADP1 on ferulate in higher pH, which favors deprotonation of weak acids.

151 **2.3. Genome sequencing of the evolved strains**

152 Whole genome sequencing was performed to discover the mutations in the evolved isolates. The
153 sequencing reads from the five sequenced strains (ASA500, ASA501, ASA502, ASA503, and WT
154 ADP1) were mapped to the reference genome of *A. baylyi* ADP1 (GenBank: CR543861). As some
155 sequence variants that differ from the reference genome are present in the parent strain WT ADP1
156 (Table S3), these variants were subtracted from the mutation pool of the evolved isolates. All the
157 mutations in the evolved isolates are summarized in Table 1. The number of mutations in coding
158 and non-coding regions for each strain is summarized in Figure 2. As ASA502 and ASA503 were
159 isolated from the same population, they shared several mutations. For all the evolved strains, many
160 of the mutations were found in the genes whose products are membrane proteins or involved in
161 cell envelope modification. Notably, some of these genes are associated with aromatic transport,
162 including *hcaE*, *vanK*, and *hcaK* (34, 36, 37). The gene *hcaE* encodes an outer membrane porin,
163 and both *vanK* and *hcaK* encode transport proteins belonging to the major facilitator superfamily.
164 The gene *hcaE* was mutated in all the four strains: insertion of the IS (insertion sequence) element,
165 *IS1236*, for ASA500 and ASA501, and a single nucleotide insertion for ASA502 and ASA503.
166 An 1137 bp deletion extending from the position 732 bp upstream of *vanK* to its CDS position 405
167 was identified in ASA500, and a 5 bp deletion in *hcaK* was identified in ASA501. All the mutations
168 in the three genes would likely result in loss of protein function.

169 We analyzed the emergence of the IS insertion in *hcaE* and the 1137 bp deletion in *vanK* by PCR-
170 amplification of the target regions from the genomes of samples from the evolving populations
171 taken at different times during the experiments. It was found that the *hcaE* mutation had already

172 emerged on day 3 (\approx 11 generations, ferulate concentration = 45 mM) for both G1 and G2 evolution
173 lines (Figure 3A). Considering that the *hcaE* mutations in the two independently evolved strains,
174 ASA500 and ASA501, are identical, the *hcaE* mutations were probably from the same origin and
175 had already occurred in the pre-culture stage where 45 mM ferulate was applied (Figure S1). The
176 deletion in the *vanK* region had already occurred in the G1 evolution line on day 20 (\approx 119
177 generations, ferulate concentration = 80 mM) and had been fixed between day 40 (\approx 236
178 generations, ferulate concentration = 115 mM) and day 50 (\approx 299 generations, ferulate
179 concentration = 120 mM) (Figure 3B).

180 Other mutations that were likely to cause loss of function were found in the genes *ACIAD2265*,
181 *iscR*, *gacA*, and *ACIAD0602* (Table 1). *ACIAD2265*, which was mutated in ASA501, is predicted
182 to encode a lytic transglycosylase involved in cell wall organization. The other genes, *iscR*, *gacA*,
183 and *ACIAD0602*, were found to be mutated in ASA502 and ASA503. *iscR* potentially encodes a
184 repressor of the *iscRSUA* operon, which is involved in the assembly of Fe-S clusters. Fe-S clusters
185 are important in enzymes for aromatic compound degradation; for example, they act as co-factors
186 of a two-component vanillate demethylase (VanAB) for the conversion of vanillate into
187 protocatechuate (38). The gene *gacA* encodes a response regulator whose deletion has been
188 characterized in *A. baumannii* and would lead to up/down-regulation of a large number of genes
189 (39). Interestingly, further analysis of the up/down-regulated genes showed that some genes are
190 related to aromatic catabolism and uptake. *ACIAD0602* encodes a putative glycosyltransferase
191 which shares >80% amino acid identity with GtrOC4 in *A. baumannii* by NCBI protein blast.
192 GtrOC4 was proposed to be involved in the outer core synthesis of lipo-oligosaccharides (40).

193 Besides the aforementioned IS1236 insertion in *hcaE* in ASA500 and ASA501, IS1236 insertion
194 was also identified in two non-coding regions in ASA502 and ASA503 (Table 1): one is 21 bp

195 upstream of *ACIAD2867*, and another one is 135 bp upstream of *ACIAD0481*. Consistent with the
196 previous report (41), all the *IS1236* insertions generated a small duplication, which resulted in 3
197 bp repeats flanking the inserted IS element, as is known to occur for the mechanism of its
198 transposition.

199 **2.4. IS-involved gene duplication was identified in the evolved strains**

200 Gene duplication was found in the evolved strains ASA500 and ASA503, which was probably
201 mediated by *IS1236*. Sequencing analysis showed that the strains ASA500 and ASA503 had DNA
202 regions at similar genomic positions with sequencing coverages 2-fold higher than those of the
203 genomes (Figure S5 and Table S4), suggesting a duplication event. The region in ASA500 had a
204 size of approximately 28 kb covering the whole coding sequences of the genes from *ACIAD3457*
205 to *ACIAD3481*, while the region in ASA503 had a size of about 33 kb extending from *ACIAD3459*
206 to *ACIAD3486* (Table S4). Most of the involved genes were shared by the duplicated regions in
207 ASA500 and ASA503. However, these genes are either not explicitly related to aromatic
208 metabolism or not well characterized. The sequence of *IS1236* was found at each junction of the
209 region (Figure S6), suggesting that the duplicated region was flanked by *IS1236*. In addition, the
210 original DNA sequences were present at the junction sites (Figure S6), indicating that the genomic
211 context of the original copy of the duplicated region was not changed; junctions between the
212 duplicated region and other locations of the genome were not found. Thus, one possibility is that
213 the region could be duplicated in the form of a composite transposon that might be inserted in one
214 of the original *IS1236* sites. The duplications in the two strains were not identical, indicating that
215 they resulted from independent events. However, the duplication was absent in ASA502, which
216 was isolated from the same population as ASA503.

217 **2.5 Rapid selection of advantageous mutations and reverse engineering**

218 To select and reverse-engineer the mutations that confer significantly improved tolerance towards
219 ferulate, a novel approach (Rapid Advantageous Mutation ScrEening and Selection, RAMSES,
220 Figure 4) was implemented. This method is based on ADP1's natural transformation, active
221 homologous recombination machinery, and efficient enrichment of advantageous mutants under

222 selective conditions. As illustrated in figure 4, the transformation is done by simply adding the
223 amplified mutated alleles containing flanking regions of sequence identity to the chromosome to
224 the cell culture (for liquid medium transformation) or the colony (for solid medium transformation).
225 The cultures after transformation are then used to inoculate different selective media with
226 incremental selective pressures (here 20 mM, 40 mM, 60 mM, and 80 mM ferulate; 40 mM, 60
227 mM, 80 mM, and 100 mM vanillate). The use of a range of selective pressures enables finding a
228 suitable condition for selection. The advantageous mutations are selected if the cells transformed
229 with the corresponding alleles show significantly improved growth under the conditions used for
230 growth.

231 We focused on the evolved isolates from the G evolution lines, ASA500 and ASA501, and
232 performed RAMSES with seven mutated alleles from them, including the *pcaU500* (P250L),
233 *hcaE500* (frameshift by IS insertion), *vanK500* (loss of function by deletion), *hcaK501*
234 (frameshift), *ACIAD2867_500* (A247V), *ACIAD2265_501* (frameshift), and *ACIAD0482_500*
235 (Δ 166-169 in amino acid sequence). These mutations were expected to have effects on ferulate
236 tolerance. The transposon-free *A. baylyi* ADP1 (42), designated as ISx, was used as the background
237 strain for the RAMSES. The strain, in which all the six copies of *IS1236* were deleted, has been
238 shown to exhibit a more stable phenotype and increased transformability (42). The transformation
239 was performed in liquid medium. The transformed cells were transferred to the selective media
240 containing 20 mM, 40 mM, 60 mM, and 80 mM ferulate. At 60 mM of ferulate, the cells
241 transformed with *hcaE500* and *hcaK501* showed evident benefit, and their growth curves could be
242 clearly distinguished from those of the controls (Figure 5), indicating the significance of the *hcaE*
243 and *hcaK* mutations. The benefit from the mutation in *hcaE* is consistent with the observation that
244 *hcaE* was mutated in all four evolved isolates. The other mutated alleles, such as the *pcaU500* and

245 *ACIAD0482_500* mutations, showed detectable but less prominent effects or large variances
246 between replicates.

247 Although the mutation-transformed cells could be directly isolated from the initial screening
248 experiment, we confirmed the reproducibility of the method by re-introducing the mutations to the
249 ISx strain by solid medium transformation. As the *hcaE* mutation found in ASA500/ASA501
250 occurred in the early stage of the G evolution lines (Figure 3A), it was chosen as the first mutation
251 to be introduced into ISx. ISx showed improved growth at the elevated ferulate concentration (20
252 mM) after being transformed with *hcaE500* (Figure 6A). An additional round of cultivation under
253 the selection condition was performed to further enrich the *hcaE* mutant. PCR analysis from the
254 genome of the enriched population showed the existence of both wild-type and the mutated *hcaE*
255 genotypes (Figure 6A), indicating the enrichment of the *hcaE* mutant. The pure strain containing
256 the mutant *hcaE* was further isolated and designated as ASA504. The mutated allele *vanK500* was
257 also chosen to transform ISx, given its propagation in the G1 evolution population over time
258 (Figure 3B) and the role of the gene related to aromatic transport (36). However, only one of the
259 two replicate populations that were transformed with *vanK500* showed improved growth and
260 enrichment of the *vanK* mutant (Figure S7). The pure strain containing *vanK500* was further
261 isolated and designated as ASA505.

262 We next used ASA504 (reconstructed mutant *hcaE*) as the parent strain for the introduction of
263 other mutated alleles, including *vanK500*, *hcaK501*, *pcaU500*, and *ACIAD0482_500*. The
264 ASA504 populations transformed with *vanK500* and *pcaU500* respectively did not show
265 significantly improved growth at the ferulate concentrations tested (20-80 mM) (data not shown).
266 However, it was found that ASA504 had poor growth on vanillate, while ASA505 (reconstructed
267 mutant *vanK*) had improved growth in the same condition (Figure S8). Therefore, we hypothesized

268 that *vanK500* would restore the growth of ASA504 on vanillate. Next, we transformed ASA504
269 with *vanK500* and used vanillate as the selective pressure for mutant enrichment. As expected, the
270 population of ASA504 showed improved growth on vanillate after being provided with the
271 *vanK500* (Figure 6B). PCR analysis of *vanK* from the genomic DNA extracted from the enriched
272 population showed only the band of *vanK500* (Figure 6B), indicating the predominance of this
273 allele. A streak-purified isolate was designated as ASA506. Transforming ASA504 with *hcaK501*
274 and *ACIAD0482_500* led to improved growth at 60 mM of ferulate (Figure 6C). After further
275 enrichment with the same selective pressure, pure isolates were obtained from each of the
276 populations. Six isolates from the *hcaK501* transformed-population and five isolates from the
277 *ACIAD0482_500* transformed-population were analyzed by Sanger sequencing for *hcaK* and
278 *ACIAD0482* respectively. All these isolates were shown to contain the corresponding mutated
279 alleles (Figure 6C). The mutation in *hcaK501* would result in a frameshift (based on the HcaK
280 sequence from UniProt entry Q7X0E0) and likely caused loss of protein function, while the
281 mutation in *ACIAD0482_500* would lead to deletion of 4 amino acids. The resulting mutants are
282 designated as ASA507 and ASA508 respectively. All the reconstructed strains were summarized
283 in Figure 6D.

284 **2.6. Characterization of the reconstructed strains**

285 To compare the growth on ferulate between the reconstructed strains, they were cultivated at
286 different ferulate concentrations. WT ADP1, ISx, ASA500 (evolved isolate), and ASA501
287 (evolved isolate) were also cultivated for comparison. Although WT ADP1 seems to differ from
288 ISx only in the copy number of the *IS1236* element, it had a better growth than ISx at 20 mM
289 ferulate (Figure 7). Compared to the reference strain ISx, the single mutants, ASA504
290 (reconstructed mutant *hcaE*) and ASA505 (reconstructed mutant *vanK*), showed improved growth

291 at 20 mM of ferulate (Figure 7). Both strains exhibited improved tolerance also towards *p*-
292 coumarate (Figure S8). However, the growth of the two single mutants was strongly inhibited at
293 40 mM ferulate. Introduction of *vanK500* only slightly improved the growth of ASA504, as
294 indicated by the growth of ASA506 (reconstructed mutant *hcaE* and *vanK*) (Figure 7). This result
295 was consistent with the previous failed attempt to enrich the *hcaE* and *vanK* double mutant using
296 ferulate. However, the growth of ASA504 on vanillate was significantly improved by introducing
297 *vanK500* (Figure S8). The genes *vanK* and *vanP* may be under the control of the same promoter
298 due to their proximity. The mutation in *vanK500* would likely cause loss of *vanK* promoter region,
299 which may negatively affect the expression of the downstream gene *vanP*. It was further explored
300 (see Supplemental Note) whether deletion of both *vanK* and *vanP*, or *vanP* alone had the same
301 effect as the mutation in *vanK500* in terms of improving the tolerance of ASA504 to vanillate.
302 Both the *hcaK* and the *ACIAD0482* mutations further improved the tolerance of ASA504 to
303 ferulate, as indicated by the robust growth of ASA507 (reconstructed mutant *hcaE* and *hcaK*) and
304 ASA508 (reconstructed mutant *hcaE* and *ACIAD0482*) at 40 mM (Figure 7). ASA507 had the best
305 growth on ferulate among the reconstructed strains, as it was the only reconstructed strain that
306 grew robustly at 60 mM ferulate. Although a direct comparison between the evolved strain
307 ASA500/ASA501 and ASA507 is complicated by their derivations from different parent strains,
308 it is clear that there is potential to further recapitulate the evolved tolerance patterns by introducing
309 other mutations.

310 **3. Discussion**

311 Lignocellulose biorefining has been demonstrated as a sustainable method for the production of
312 fuels, chemicals, and materials (43). To date, the polysaccharide fraction of lignocellulose is of
313 primary interest for the downstream conversion, whereas the lignin fraction is usually regarded as

314 a waste, a low value-added product, or a source for process heat. Recent analysis has indicated that
315 lignin valorization is essential to increase the sustainability and economic viability of
316 lignocellulose-based industries (44, 45). The success of lignin valorization largely relies on lignin
317 depolymerization and subsequent upgrading of the heterogeneous lignin-derived aromatics (44).
318 However, due to the heterogeneity and impurity of lignin, it is a very challenging feedstock for
319 chemical processes (29). The microbial valorization of lignin has been suggested (25, 27, 29); the
320 aromatic catabolic pathways in some microbes allow the “funneling” of various aromatic species
321 into two key aromatic ring-cleavage substrates, commonly protocatechuate and catechol, which
322 can be further channeled to central carbon metabolism. Salvachúa *et al.* examined fourteen bacteria
323 for their ability to utilize a lignin-enriched substrate (26); *A. baylyi* ADP1 was the best among the
324 tested bacteria both to degrade high molecular weight lignin and consume low molecular weight
325 lignin-derived compounds. The use of *A. baylyi* ADP1 as a host of engineering for biological lignin
326 valorization is further warranted by its straightforward genome editing (14, 46) and the rapidly
327 increasing number of available genetic tools (46).

328 Apart from the availability of lignin-derived aromatics for use as a substrate, their toxicity must
329 be considered, which is regarded as a major challenge in the biological upgrading of lignin-
330 enriched streams (47, 48). All the aromatic compounds tested in the current study showed varying
331 degrees of toxicity when used as sole carbon sources: the growth of wild-type ADP1 on ferulate
332 was significantly impaired when the concentration was increased from 20 mM to 40 mM.
333 Moreover, 80 mM was lethal to the cells, and cell growth was not observed in 20 mM *p*-coumarate
334 (Figure 1B). In a previous study, a 33% reduction of growth rate was observed in glucose-grown
335 *Pseudomonas putida* KT2440 and *Escherichia coli* MG1655 in the presence of 61 mM and 30 mM
336 *p*-coumarate respectively (49). Consequently, the use of batch fermentation is greatly limited, and

337 suitable fed-batch strategies need to be developed for substrate feeding without reaching toxicity
338 limits. Some aromatics can cause severe growth impairment at much lower concentrations. For
339 example, benzoate and catechol have been reported to completely inhibit glucose-grown *P. putida*
340 KT2440 at 50 mM and 8 mM respectively (47, 50). In addition, prolonged contact with toxic
341 aromatic compounds, even at low concentrations, may lead to other cellular malfunctions, such as
342 cellular energy shortage, as demonstrated by Kohlstedt *et al.* (47). Biotransformation can become
343 more challenging when the lignin-derived aromatics serve as the sole carbon sources, especially if
344 the products of interest require high levels of carbon substrate to sustain the synthesis of desired
345 products.

346 In our attempts to discover the tolerance mechanisms behind the evolved strains, aromatic-specific
347 transport was found to play an important role. The loss-of-function mutations in the genes *hcaE*,
348 *hcaK*, and *vanK* were identified to be advantageous by RAMSES. Reconstruction of the *hcaE*
349 mutation improved the tolerance towards both ferulate and *p*-coumarate. This gene encodes an
350 outer membrane porin, and it clusters with other genes responsible for ferulate and *p*-coumarate
351 catabolism (34), implying that the porin may act on hydroxycinnamates. Interestingly, the *hcaE*
352 mutation resulted in decreased tolerance towards vanillate. HcaE might have a low specificity for
353 vanillate. The tolerance towards vanillate was improved by reconstruction of the *vanK* mutation.
354 The gene *vanK* encodes a transporter belonging to the major facilitator superfamily. Its location
355 near the *vanAB* operon, which is responsible for vanillate catabolism, implies that vanillate may
356 be transported by VanK, as proposed previously (51). VanK has been also reported to mediate the
357 uptake of two other intermediates in the aromatic catabolic pathway, protocatechuate and *p*-
358 hydroxybenzoate (36). The combination of the *hcaE* and *hcaK* mutations further improved the
359 tolerance to ferulate. The gene *hcaK*, transcribed in the opposite direction of the *hca* operon by a

360 bidirectional promoter (52), encodes a transporter which also belongs to the major facilitator
361 superfamily. It is possible that ferulate and *p*-coumarate are both transported by HcaK. Loss of
362 function mutations in these genes related to aromatic acid transport suggests a mechanism for
363 tolerance/growth improvement by reducing the entry of aromatics. This is in line with a previous
364 study in *P. putida* (9), which showed that deletion of an outer membrane porin PP_3350 in a wild-
365 type strain decreased the lag phase in 20 g/L *p*-coumarate (~123 mM) by >30 hours. In a recent
366 study, Kusumawardhani *et al.* elucidated that several genes associated with porins and transport
367 proteins were downregulated in an ALE-derived toluene-tolerant *P. putida* S12 (53). Besides the
368 machinery associated with molecule uptake, efflux pumps have also been shown to contribute to
369 the tolerance towards aromatic compounds (9, 49, 53). It is commonly known that aromatic
370 compounds can disrupt cell membrane integrity due to their lipophilic (or partially lipophilic)
371 nature (54, 55) and are also suggested to exert toxic effects intracellularly through different modes
372 of actions (55, 56). Therefore, this mechanism of tolerance against aromatic compounds may result
373 from their toxic effects in the periplasm or cytoplasm. In nature, the aromatic transport systems
374 can be important for nutrient uptake, but in concentrations relevant to applications, their role
375 becomes less important since aromatic acids in their protonated form can diffuse down the
376 concentration gradient across cell membranes (35, 56). This may also explain our observation that
377 wild-type ADP1 showed improved growth on ferulate at a higher pH, which can promote
378 deprotonation and decrease the proportion of permeable aromatic acids.

379 The mutation in *ACIAD0482* was surprisingly found to be advantageous in ferulate tolerance. The
380 product of *ACIAD0482* has not been reported in *A. baylyi* but has homology to LpsB of
381 *Acinetobacter baumannii* with >80% identity. LpsB was reported to be a glycosyltransferase of
382 the lipopolysaccharide (LPS) core (57). The 12 bp deletion in *ACIAD0482* would lead to the

383 deletion of four amino acids from position 166 to 169 in the protein sequence. However, the effect
384 of the deletion on the protein function is yet to be explored. Interestingly, another gene that is
385 associated with lipooligosaccharide (LOS) was found to be mutated in ASA502 and ASA503: a
386 single nucleotide deletion in *ACIAD0602*, which may lead to loss of protein function. *ACIAD0602*
387 encodes a putative glycosyltransferase sharing >80% identity with GtrOC4 in *A. baumannii*, and
388 GtrOC4 was proposed to be involved in the synthesis of the outer core of LOS (40). LPS/LOS is
389 known to provide a barrier protecting gram-negative bacteria from hydrophobic substances (58,
390 59), but the mechanism of the tolerance improvement by the glycosyltransferase mutation remains
391 unclear.

392 The *IS1236* element played an important role in the mutation development of the evolution
393 experiment presented here. In addition to its insertion in *hcaE* in ASA500/ASA501, *IS1236* was
394 found to be inserted in two non-coding regions in the strain ASA502 and ASA503. Interestingly,
395 the gene duplications observed in ASA500 and ASA503 were found to be related to *IS1236*; the
396 duplicated region was flanked by *IS1236*, but the genomic context of the original copy of the
397 region seemed not to change. In addition, junctions between the duplicated region and other
398 locations of the genome were not found. One possibility is that the duplication may result from the
399 formation of a new composite transposon by *IS1236* flanking the duplicated region, followed by
400 integration of the composite transposon into one of the *IS1236* sites. Although the duplications in
401 the two strains originated from independent evolution events, and most of the duplicated genes
402 were shared by the two strains, the roles of the duplications are not obvious. Because the strain
403 ASA502, which was from the same population and shared many common mutations with ASA503,
404 only showed a slight difference from ASA503 in the growth on ferulate but did not carry the
405 duplication. In addition, the genes in the duplicated region are not obviously related to aromatic

406 metabolism. Nevertheless, it cannot be excluded that they may have underlying effects on the
407 tolerance or metabolism of aromatics; for example, some of the genes may have regulatory effects
408 or encode membrane protein. *A. baylyi* ADP1 contains 6 copies of a single type of IS element,
409 IS1236, five of which are identical (60). In a previous evolution study, it was reported that IS1236
410 was responsible for 41% of mutations in ADP1 after propagation in rich nutrient broth for 1000
411 generations (61). Although IS elements may play a role in fitness improvement during evolution,
412 they can also contribute to undesired genetic instability in engineered strains (42). This prompted
413 us to use the transposon-free *A. baylyi* ADP1 (42), ISx, as the background strain for reverse
414 engineering, though it seemed to have a decreased tolerance towards ferulate compared to wild-
415 type ADP1.

416 From the point of view of rational engineering, it is desirable to find the “minimal set” of mutations
417 resulting in significant improvement of a phenotype. Here, by employing the RAMSES
418 methodology, we were rapidly able to identify and reintroduce two key mutations (the *hcaE* and
419 *hcaK* mutations) that alone significantly improved the tolerance of *A. baylyi* ADP1 towards
420 ferulate. Such a method would be particularly useful when screening a large number of mutations
421 (and their combinations), in contrast to individual construction of knock-in cassettes. The high
422 capability of screening would also make it possible to expand the subset of mutations to be tested
423 beyond the mutations that are either intuitive or convergent between ALE replicates, increasing
424 the potential to discover novel mechanisms behind the improved phenotypes. Here, for example,
425 the *ACIAD0482* mutation, which may not be considered as beneficial intuitively, was found to be
426 advantageous. Moreover, the RAMSES approach can be easily automated with the use of a liquid
427 handling robot, owing to the possibility of transforming *A. baylyi* directly in liquid culture. In
428 principle, the RAMSES approach can be used to study most types of evolved alleles that can be

429 introduced using conventional allelic replacement methods. An adaptation of the type of donor
430 DNA used for transformation also allows the study of duplication, a type of genetic change that is
431 traditionally difficult to analyze. For such a mutation type, transformation with a linear synthetic
432 bridging fragment (SBF) can recapitulate a specific duplication by providing a platform for
433 homologous recombination between sequences downstream and upstream of a target region (17).
434 SBFs can be used for the amplification of desired genes or genomic target regions and, as for other
435 types of mutations, the enrichment of duplicated transformants under selection can be informative
436 (17).

437 **4. Conclusion**

438 We exploited the natural competence and high recombination efficiency of *A. baylyi* ADP1 in
439 developing a simple and rapid method for screening, identifying, and reverse-engineering
440 advantageous mutations that arose during ALE. The method was applied on strains that were
441 evolved for high ferulate tolerance and then subjected to whole-genome sequencing. Among
442 numerous mutations, we were able to determine that mutations in *hcaE* and *hcaK* played a major
443 role in the improved tolerance. By simply introducing the combination of these two mutations in
444 a parent strain, the high tolerance against ferulate could be restored. This study highlights the
445 potential of applying the naturally competent *A. baylyi* ADP1 for evolution studies and strain
446 development and facilitates the construction of more robust cell factories for aromatic substrate
447 valorization.

448 **5. Materials and methods**

449 **2.1. Strains and media**

450 Wild-type *Acinetobacter baylyi* ADP1 (DSM 24193, DSMZ, Germany) was used as a starting
451 strain for ALE, designated as WT ADP1. The transposon-free *A. baylyi* ADP1 (42) (a kind gift
452 from Barrick lab), designated as ISx in this study, was used as the parent strain for reverse
453 engineering. *E. coli* XL1-Blue (Stratagene, USA) was used as the host in cloning steps. All the
454 strains used in this study are listed in Table 2.

455 Mineral salts medium (MSM) was used for ALE, growth study, and reverse engineering. The
456 carbon sources, including ferulate, vanillate, *p*-coumarate, casamino acids, and acetate were added
457 when appropriate. The composition of MSM was 3.88 g/l K₂HPO₄, 1.63 g/l NaH₂PO₄, 2.00 g/l
458 (NH₄)₂SO₄, 0.1 g/l MgCl₂·6H₂O, 10 mg/l Ethylenediaminetetraacetic acid (EDTA), 2 mg/l
459 ZnSO₄·7H₂O, 1 mg/l CaCl₂·2H₂O, 5 mg/l FeSO₄·7H₂O, 0.2 mg/l Na₂MoO₄·2H₂O, 0.2 mg/l
460 CuSO₄·5H₂O, 0.4 mg/l CoCl₂·6H₂O, 1 mg/l MnCl₂·2H₂O. The stock solutions of ferulate, vanillate,
461 and coumarate were prepared with a concentration of 200 mM; briefly, the proper amount of
462 aromatic acid (all purchased from Sigma, USA) was added in deionized water and dissolved by
463 slowly adding NaOH while stirring. The final pH of the stock solutions was 8.2~8.3. The stock
464 solutions were further sterilized by filtration with sterile filters (pore size 0.2 μm, Whatman). The
465 stock solutions were freshly prepared before each experiment. *E. coli* strains were maintained on
466 modified LB medium (10 g/L tryptone, 5 g/L yeast extract, 1 g/L NaCl) supplemented with 1%
467 glucose. For solid medium, 15 g/L agar was added. Spectinomycin (50 μg/ml) was added when
468 appropriate.

469 **2.2. Adaptive laboratory evolution of *Acinetobacter baylyi* ADP1**

470 Two parallel evolutions with ferulate as a sole carbon source, designated as G1 and G2 evolution
471 lines here, have been described previously (23). Here, two additional parallel evolutions were
472 carried out to improve the tolerance on ferulate, designated as T1 and T2 evolution lines, in which
473 acetate and casamino acids were supplemented in addition to ferulate. The ALE cultivation was
474 performed in Erlenmeyer flasks (100 ml) containing 10 ml medium at 30 °C and 300 rpm. Wild-
475 type ADP1 was first plated on solid MSM, and 25 mM ferulate, 10 mM acetate, and 0.2% (W/V)
476 casamino acids were supplemented. The single colony from the plate was pre-cultivated in MSM
477 supplemented with 55 mM ferulate, 10 mM acetate, and 0.2% (W/V) casamino acids. The pre-
478 culture was transferred to two Erlenmeyer flasks containing the same medium, resulting in the two
479 parallel evolution populations. The cells were transferred to fresh media before reaching the
480 stationary phase daily. The optical density at 600 nm (OD) was measured before each transfer. The
481 amount of inoculum for each transfer was adjusted so that the initial OD after each transfer was
482 between 0.03 and 0.1. The cells were cryopreserved at -80 °C every two transfers. The
483 concentration of ferulate was gradually increased during the evolution (Figure S1B): a 5 mM or
484 10 mM concentration increase was applied if the ODs before passages could be maintained at a
485 high level (> 3). Individual isolates were streak purified twice on LB-agar plates from the end
486 population of each evolution line.

487 The number of generations (n) per flask was calculated with the following equation:

$$488 \quad n = \log\left(\frac{N}{N_0}\right) / \log(2) \quad ,$$

489 where N is the final OD₆₀₀ of the culture and N₀ is the initial OD₆₀₀.

490 **2.3. Phenotype characterization**

491 The growth of different strains on different aromatic substrates was tested by cultivations in 96-
492 well plates (Greiner Bio-One™ CellStar™ µClear™). The cells were pre-cultivated in MSM
493 supplemented with 5 mM aromatic substrate (ferulate/vanillate/ *p*-coumarate) at which both the
494 evolved strains and the reference strains can grow. After overnight cultivation, the cultures were
495 inoculated (initial OD 0.05) into the media supplemented with the corresponding aromatic
496 substrate at higher concentrations (as indicated in the result section). For strains from the evolution
497 line T2, appropriate amounts of acetate and casamino acids were added when needed. The culture
498 (200 µl) was transferred to the 96-well plate and incubated in Spark multimode microplate reader
499 (Tecan, Switzerland) at 30 °C. Double orbital shaking was performed for 5 min twice an hour with
500 an amplitude of 6 mm and a frequency of 54 rpm. OD was measured every hour. The cultivations
501 were performed in duplicate. To study the effect of increased pH on cell growth, the pH of the
502 media was adjusted by adding concentrated NaOH. The media was further sterilized by filtration.
503 The cultivation was performed with the same procedure as mentioned above. For pre-cultivation,
504 the media without pH adjustment was used.

505 **2.4. Whole-genome sequencing of the evolved strains**

506 Approximately 1 µg of genomic DNA from each strain was isolated using the Nucleospin gDNA
507 cleanup kit (Macherey-Nigel), then fragmented by sonication to an average size of 300–500 bp.
508 End repair, A-tailing, and adapter ligation reactions were performed on the fragmented DNA
509 using the NEBNext Ultra II kit (New England Biolabs). Illumina paired-end sequencing was
510 performed on a NextSeq500 device at the Georgia Genomics Facility (University of Georgia).

511 The sequences were analyzed using both Geneious prime version 8.1 with default settings (62) and
512 the Breseq (version 0.35.4) computational pipeline (63). Version 2.4.1 of bowtie2 and version
513 4.0.0 of R were used in the pipeline. The consensus mode was used with the default consensus
514 frequency cutoff of 0.8 and polymorphism frequency cutoff of 0.2. The raw reads from the five
515 sequenced strains (ASA500, ASA501, ASA502, ASA503, and WT ADP1) were mapped to the
516 reference genome of *A. baylyi* ADP1 (GenBank: CR543861).

517 **2.5. Initial screening of advantageous mutations**

518 The mutated alleles were first PCR-amplified from the evolved strains with Phusion high-fidelity
519 DNA polymerase (Thermo Scientific, Finland), using the primers listed in Table 3. The amplified
520 DNA fragments contained at least 500 bp of homology on each side of the mutated region. The
521 PCR products were then loaded onto the agarose gel for electrophoresis. To avoid cross-
522 contamination between the PCR products of the different mutated alleles, it is important to leave
523 one well empty between the samples and not to overload the PCR products. The amplified DNA
524 was purified with GeneJET Gel Extraction Kit (Thermo Scientific) and eluted with pre-warmed
525 water. The concentrations of the purified PCR products ranged from 30 ng/ μ l to 100 ng/ μ l. For
526 natural transformation, ISx was first pre-cultivated in LB medium supplemented with 0.4%
527 glucose. When the cells were in early exponential phase, 20 μ l of the purified DNA was directly
528 added to 180 μ l of the culture, and then the mixture was incubated in 14 ml cultivation tube at
529 30 °C and 300 rpm for 3~4 hours. The cells treated with water, an unmutated allele (gene entry:
530 *ACIAD3383*) amplified from the evolved strain, and without any treatment were used as the
531 controls. To adapt the cells to the medium used for the downstream process, 5 ml of MSM
532 supplemented with 5 mM ferulate was added to the tube, and the culture was incubated overnight.
533 After the incubation, 10 μ l of the cells were transferred to different wells of a 96-well plate (Greiner

534 Bio-One™ CellStar™ µClear™) containing 140 µl of MSM with elevated ferulate concentrations
535 (20 mM, 40 mM, 60 mM, and 80 mM). The plate was incubated in Spark multimode microplate
536 reader (Tecan, Switzerland) at 30 °C, and the OD was measured every hour.

537 **2.6. Reverse engineering of key mutations**

538 The selected mutated alleles were PCR-amplified from the evolved strains using the primers listed
539 in Table 3, and gel-extracted. For transformation, the background strain, ISx, was first streaked on
540 LB-agar, and the plate was incubated at 30 °C overnight. The purified DNA (0.5 µl) was added
541 onto single colonies and mixed well by pipetting up and down. After overnight incubation at 30 °C,
542 the colony treated with the DNA was scraped and suspended in MSM supplemented 5 mM of the
543 corresponding aromatic substrate (ferulate or vanillate). As the control, a colony without DNA
544 treatment was subjected to the same process. The suspension was further incubated at 30 °C and
545 300 rpm for 0.5-10 h. After incubation, the suspension was used to inoculate 200 µl of MSM
546 supplemented with elevated concentrations of the aromatic substrate (ferulate: 20 mM, 40 mM, 60
547 mM, and 80 mM; vanillate: 40 mM, 60 mM, 80 mM, and 100 mM) in different wells of the 96-
548 well plate. The plate was incubated in Spark multimode microplate reader (Tecan, Switzerland) at
549 30 °C, and the OD was monitored every hour. If the cells treated with the mutated allele showed
550 improved growth over the control at the elevated aromatic concentration, 5 µl of the cells were
551 taken from the well and used to inoculate 5 ml of MSM containing the same (or higher)
552 concentration of the corresponding aromatic substrate for further mutant enrichment. The culture
553 was further streaked on LB-agar. The clones carrying the mutated allele were identified by picking
554 single colonies for PCR analysis or Sanger sequencing.

555 **2.7. Genetic engineering**

556 ASA509 was constructed by transforming ASA504 with a linear integration cassette containing
557 the spectinomycin resistance gene flanked by the sequences homologous to the sequences
558 surrounding the *vanKP* region. The cassette was constructed by overlap extension PCR with the
559 left flanking sequence (amplified with primers P1-F and P2-R, Table S2), the spectinomycin
560 resistance gene (amplified with primers spec-F and spec-R), and the right flanking sequence
561 (amplified with primers P3-F and P4-R). The linear cassette was later cloned to a previously
562 described plasmid (18), and the left flanking sequence was replaced with another flanking
563 sequence amplified with primers P5-F and P6-R. The resulting plasmid (non-replicating plasmid
564 in ADP1) was used to transform ASA504 to obtain ASA510.

565 **2.8. Analysis of substrate consumption**

566 The concentrations of ferulate, vanillate, and acetate were analyzed using Agilent Technology
567 1100 Series HPLC (UV/VIS system) equipped with G1313A autosampler, G1322A degasser,
568 G1311A pump, and G1315A DAD. Rezex RFQ-Fast Acid H+ (8%) (Phenomenex) was used as
569 the column and placed at 80 °C. Sulfuric acid (0.005 N) was used as the eluent with a pumping
570 rate of 0.8 ml/min.

571 **Data availability**

572 Next-generation sequencing data generated in this study are available in NCBI Sequence Read
573 Archive (SRA) BioProject accession number: PRJNA761218.

574 **Acknowledgements**

575 Funding: The research work was supported by Academy of Finland (grants no. 310188, 334822),
576 Novo Nordisk Foundation (grant no. NNF21OC0067758) and U.S. Department of Agriculture
577 (grant no. 2018-67009-27926).

578 **Author contribution**

579 Author contribution: JL, SS, and VS designed the study. JL and EM carried out the research
580 work. JL, EM, and SB analyzed the data. SS, EN, and VS supervised the study. All authors
581 participated in writing the manuscript.

582 **References**

- 583 1. Dragosits M, Mattanovich D. 2013. Adaptive laboratory evolution – principles and applications
584 for biotechnology. *Microb Cell Fact* 12:64.
- 585 2. Sandberg TE, Salazar MJ, Weng LL, Palsson BO, Feist AM. 2019. The emergence of adaptive
586 laboratory evolution as an efficient tool for biological discovery and industrial biotechnology.
587 *Metab Eng* 56:1–16.
- 588 3. Fletcher E, Feizi A, Bisschops MMM, Hallström BM, Khoomrung S, Siewers V, Nielsen J. 2017.
589 Evolutionary engineering reveals divergent paths when yeast is adapted to different acidic
590 environments. *Metab Eng* 39:19–28.
- 591 4. Kildegaard KR, Hallström BM, Blicher TH, Sonnenschein N, Jensen NB, Sherstyk S, Harrison SJ,
592 Maury J, Herrgård MJ, Juncker AS, Forster J, Nielsen J, Borodina I. 2014. Evolution reveals a
593 glutathione-dependent mechanism of 3-hydroxypropionic acid tolerance. *Metab Eng* 26:57–66.
- 594 5. Mundhada H, Seoane JM, Schneider K, Koza A, Christensen HB, Klein T, Phaneuf P V., Herrgård M,

- 595 Feist AM, Nielsen AT. 2017. Increased production of L-serine in *Escherichia coli* through Adaptive
596 Laboratory Evolution. *Metab Eng* 39:141–150.
- 597 6. Almario MP, Reyes LH, Kao KC. 2013. Evolutionary engineering of *Saccharomyces cerevisiae* for
598 enhanced tolerance to hydrolysates of lignocellulosic biomass. *Biotechnol Bioeng* 110:2616–
599 2623.
- 600 7. Lim HG, Fong B, Alarcon G, Magurudeniya HD, Eng T, Szubin R, Olson CA, Palsson BO, Gladden
601 JM, Simmons BA, Mukhopadhyay A, Singer SW, Feist AM. 2020. Generation of ionic liquid
602 tolerant *Pseudomonas putida* KT2440 strains via adaptive laboratory evolution. *Green Chem*
603 22:5677–5690.
- 604 8. Phaneuf P V., Yurkovich JT, Heckmann D, Wu M, Sandberg TE, King ZA, Tan J, Palsson BO, Feist
605 AM. 2020. Causal mutations from adaptive laboratory evolution are outlined by multiple scales of
606 genome annotations and condition-specificity. *BMC Genomics* 21:514.
- 607 9. Mohamed ET, Werner AZ, Salvachúa D, Singer CA, Szostkiewicz K, Rafael Jiménez-Díaz M, Eng T,
608 Radi MS, Simmons BA, Mukhopadhyay A, Herrgård MJ, Singer SW, Beckham GT, Feist AM. 2020.
609 Adaptive laboratory evolution of *Pseudomonas putida* KT2440 improves p-coumaric and ferulic
610 acid catabolism and tolerance. *Metab Eng Commun* 11:e00143.
- 611 10. Lee D-H, Palsson BØ. 2010. Adaptive Evolution of *Escherichia coli* K-12 MG1655 during Growth on
612 a Nonnative Carbon Source, l-1,2-Propanediol. *Appl Environ Microbiol* 76:4158–4168.
- 613 11. Atsumi S, Wu T, Machado IMP, Huang W, Chen P, Pellegrini M, Liao JC. 2010. Evolution, genomic
614 analysis, and reconstruction of isobutanol tolerance in *Escherichia coli*. *Mol Syst Biol* 6:449.
- 615 12. Neidle EL, Ornston LN. 1986. Cloning and expression of *Acinetobacter calcoaceticus* catechol 1,2-
616 dioxygenase structural gene *catA* in *Escherichia coli*. *J Bacteriol* 168:815–820.

- 617 13. Santala S, Santala V. 2021. *Acinetobacter baylyi* ADP1—naturally competent for synthetic
618 biology. *Essays Biochem*.
- 619 14. de Berardinis V, Vallenet D, Castelli V, Besnard M, Pinet A, Cruaud C, Samair S, Lechaplais C,
620 Gyapay G, Richez C, Durot M, Kreimeyer A, Le Fèvre F, Schächter V, Pezo V, Döring V, Scarpelli C,
621 Médigue C, Cohen GN, Marlière P, Salanoubat M, Weissenbach J. 2008. A complete collection of
622 single-gene deletion mutants of *Acinetobacter baylyi* ADP1. *Mol Syst Biol* 4:174.
- 623 15. Santala V, Karp M, Santala S. 2016. Bioluminescence-based system for rapid detection of natural
624 transformation. *FEMS Microbiol Lett* 363:fnw125.
- 625 16. Jiang X, Palazzotto E, Wybraniec E, Munro LJ, Zhang H, Kell DB, Weber T, Lee SY. 2020.
626 Automating Cloning by Natural Transformation. *ACS Synth Biol* 9:3228–3235.
- 627 17. Tumen-Velasquez M, Johnson CW, Ahmed A, Dominick G, Fulk EM, Khanna P, Lee SA, Schmidt AL,
628 Linger JG, Eiteman MA, Beckham GT, Neidle EL. 2018. Accelerating pathway evolution by
629 increasing the gene dosage of chromosomal segments. *Proc Natl Acad Sci* 115:7105–7110.
- 630 18. Santala S, Efimova E, Kivinen V, Larjo A, Aho T, Karp M, Santala V. 2011. Improved Triacylglycerol
631 Production in *Acinetobacter baylyi* ADP1 by Metabolic Engineering. *Microb Cell Fact* 10:36.
- 632 19. Lehtinen T, Efimova E, Santala S, Santala V. 2018. Improved fatty aldehyde and wax ester
633 production by overexpression of fatty acyl-CoA reductases. *Microb Cell Fact* 17:19.
- 634 20. Salmela M, Lehtinen T, Efimova E, Santala S, Santala V. 2019. Alkane and wax ester production
635 from lignin related aromatic compounds. *Biotechnol Bioeng* bit.27005.
- 636 21. Luo J, Efimova E, Losoi P, Santala V, Santala S. 2020. Wax ester production in nitrogen-rich
637 conditions by metabolically engineered *Acinetobacter baylyi* ADP1. *Metab Eng Commun*
638 10:e00128.

- 639 22. Santala S, Santala V, Liu N, Stephanopoulos G. 2021. Partitioning metabolism between growth
640 and product synthesis for coordinated production of wax esters in *Acinetobacter baylyi* ADP1.
641 *Biotechnol Bioeng*.
- 642 23. Luo J, Lehtinen T, Efimova E, Santala V, Santala S. 2019. Synthetic metabolic pathway for the
643 production of 1-alkenes from lignin-derived molecules. *Microb Cell Fact* 18:48.
- 644 24. Arvay E, Biggs BW, Guerrero L, Jiang V, Tyo K. 2021. Engineering *Acinetobacter baylyi* ADP1 for
645 mevalonate production from lignin-derived aromatic compounds. *Metab Eng Commun*
646 13:e00173.
- 647 25. Vardon DR, Franden MA, Johnson CW, Karp EM, Guarnieri MT, Linger JG, Salm MJ, Strathmann
648 TJ, Beckham GT. 2015. Adipic acid production from lignin. *Energy Environ Sci* 8:617–628.
- 649 26. Salvachúa D, Karp EM, Nimlos CT, Vardon DR, Beckham GT. 2015. Towards lignin consolidated
650 bioprocessing: simultaneous lignin depolymerization and product generation by bacteria. *Green*
651 *Chem* 17:4951–4967.
- 652 27. Linger JG, Vardon DR, Guarnieri MT, Karp EM, Hunsinger GB, Franden MA, Johnson CW, Chupka
653 G, Strathmann TJ, Pienkos PT, Beckham GT. 2014. Lignin valorization through integrated
654 biological funneling and chemical catalysis. *Proc Natl Acad Sci*.
- 655 28. Abdelaziz OY, Brink DP, Prothmann J, Ravi K, Sun M, García-Hidalgo J, Sandahl M, Hulteberg CP,
656 Turner C, Lidén G, Gorwa-Grauslund MF. 2016. Biological valorization of low molecular weight
657 lignin. *Biotechnol Adv* 34:1318–1346.
- 658 29. Beckham GT, Johnson CW, Karp EM, Salvachúa D, Vardon DR. 2016. Opportunities and challenges
659 in biological lignin valorization. *Curr Opin Biotechnol* 42:40–53.
- 660 30. Harwood CS, Parales RE. 1996. The β -keto adipate Pathway and the Biology of Self-identity. *Annu*

- 661 Rev Microbiol 50:553–590.
- 662 31. Fischer R, Bleichrodt FS, Gerischer UC. 2008. Aromatic degradative pathways in *Acinetobacter*
663 baylyi underlie carbon catabolite repression. *Microbiology* 154:3095–3103.
- 664 32. Seaton SC, Neidle EL. 2018. Chapter 10. Using Aerobic Pathways for Aromatic Compound
665 Degradation to Engineer Lignin Metabolism, p. 252–289. *In* .
- 666 33. Pardo I, Jha RK, Bermel RE, Bratti F, Gaddis M, McIntyre E, Michener W, Neidle EL, Dale T,
667 Beckham GT, Johnson CW. 2020. Gene amplification, laboratory evolution, and biosensor
668 screening reveal MucK as a terephthalic acid transporter in *Acinetobacter baylyi* ADP1. *Metab*
669 *Eng* 62:260–274.
- 670 34. Smith MA, Weaver VB, Young DM, Ornston LN. 2003. Genes for Chlorogenate and
671 Hydroxycinnamate Catabolism (hca) Are Linked to Functionally Related Genes in the dca-pca-qui-
672 pob-hca Chromosomal Cluster of *Acinetobacter* sp. Strain ADP1. *Appl Environ Microbiol* 69:524–
673 532.
- 674 35. Nichols NN, Harwood CS. 1997. PcaK, a high-affinity permease for the aromatic compounds 4-
675 hydroxybenzoate and protocatechuate from *Pseudomonas putida*. *J Bacteriol* 179:5056–5061.
- 676 36. D’Argenio DA, Segura A, Coco WM, Bünz P V., Ornston LN. 1999. The Physiological Contribution
677 of *Acinetobacter* PcaK, a Transport System That Acts upon Protocatechuate, Can Be Masked by
678 the Overlapping Specificity of VanK. *J Bacteriol* 181:3505–3515.
- 679 37. Parke D, Ornston LN. 2003. Hydroxycinnamate (hca) Catabolic Genes from *Acinetobacter* sp.
680 Strain ADP1 Are Repressed by HcaR and Are Induced by Hydroxycinnamoyl-Coenzyme A
681 Thioesters. *Appl Environ Microbiol* 69:5398–5409.
- 682 38. Morawski B, Segura A, Ornston LN. 2000. Substrate Range and Genetic Analysis of *Acinetobacter*

- 683 Vanillate Demethylase. *J Bacteriol* 182:1383–1389.
- 684 39. Cerqueira GM, Kostoulias X, Khoo C, Aibinu I, Qu Y, Traven A, Peleg AY. 2014. A Global Virulence
685 Regulator in *Acinetobacter baumannii* and Its Control of the Phenylacetic Acid Catabolic Pathway.
686 *J Infect Dis* 210:46–55.
- 687 40. Kenyon JJ, Nigro SJ, Hall RM. 2014. Variation in the OC Locus of *Acinetobacter baumannii*
688 Genomes Predicts Extensive Structural Diversity in the Lipooligosaccharide. *PLoS One* 9:e107833.
- 689 41. Gerischer U, D'Argenio DA, Ornston LN. 1996. IS 1236, a newly discovered member of the IS3
690 family, exhibits varied patterns of insertion into the *Acinetobacter calcoaceticus* chromosome.
691 *Microbiology* 142:1825–1831.
- 692 42. Suárez GA, Renda BA, Dasgupta A, Barrick JE. 2017. Reduced Mutation Rate and Increased
693 Transformability of Transposon-Free *Acinetobacter baylyi* ADP1-ISx. *Appl Environ Microbiol* 83.
- 694 43. Ragauskas AJ. 2006. The Path Forward for Biofuels and Biomaterials. *Science* (80-) 311:484–489.
- 695 44. Schutyser W, Renders T, Van den Bosch S, Koelewijn S-F, Beckham GT, Sels BF. 2018. Chemicals
696 from lignin: an interplay of lignocellulose fractionation, depolymerisation, and upgrading. *Chem*
697 *Soc Rev* 47:852–908.
- 698 45. Ragauskas AJ, Beckham GT, Biddy MJ, Chandra R, Chen F, Davis MF, Davison BH, Dixon RA, Gilna
699 P, Keller M, Langan P, Naskar AK, Saddler JN, Tschaplinski TJ, Tuskan GA, Wyman CE. 2014. Lignin
700 Valorization: Improving Lignin Processing in the Biorefinery. *Science* (80-) 344:1246843–
701 1246843.
- 702 46. Biggs BW, Bedore SR, Arvay E, Huang S, Subramanian H, McIntyre EA, Duscent-Maitland C V.,
703 Neidle EL, Tyo KEJ. 2020. Development of a genetic toolset for the highly engineerable and
704 metabolically versatile *Acinetobacter baylyi* ADP1. *Nucleic Acids Res* 48:5169–5182.

- 705 47. Kohlstedt M, Starck S, Barton N, Stolzenberger J, Selzer M, Mehlmann K, Schneider R, Pleissner D,
706 Rinkel J, Dickschat JS, Venus J, B.J.H. van Duuren J, Wittmann C. 2018. From lignin to nylon:
707 Cascaded chemical and biochemical conversion using metabolically engineered *Pseudomonas*
708 *putida*. *Metab Eng* 47:279–293.
- 709 48. Salvachúa D, Johnson CW, Singer CA, Rohrer H, Peterson DJ, Black BA, Knapp A, Beckham GT.
710 2018. Bioprocess development for muconic acid production from aromatic compounds and
711 lignin. *Green Chem* 20:5007–5019.
- 712 49. Calero P, Jensen SI, Bojanovič K, Lennen RM, Koza A, Nielsen AT. 2018. Genome-wide
713 identification of tolerance mechanisms toward *p*-coumaric acid in *Pseudomonas putida*.
714 *Biotechnol Bioeng* 115:762–774.
- 715 50. van Duuren JBJH, Wijte D, Karge B, Martins dos Santos VAP, Yang Y, Mars AE, Eggink G. 2012. pH-
716 stat fed-batch process to enhance the production of *cis*, *cis*-muconate from benzoate by
717 *Pseudomonas putida* KT2440-JD1. *Biotechnol Prog* 28:85–92.
- 718 51. Pernstich C, Senior L, MacInnes KA, Forsaith M, Curnow P. 2014. Expression, purification and
719 reconstitution of the 4-hydroxybenzoate transporter PcaK from *Acinetobacter* sp. ADP1. *Protein*
720 *Expr Purif* 101:68–75.
- 721 52. Kim Y, Joachimiak G, Bigelow L, Babnigg G, Joachimiak A. 2016. How Aromatic Compounds Block
722 DNA Binding of HcaR Catabolite Regulator. *J Biol Chem* 291:13243–13256.
- 723 53. Kusumawardhani H, Furtwängler B, Blommestijn M, Kaltenyť A, van der Poel J, Kolk J, Hosseini
724 R, de Winde JH. 2021. Adaptive Laboratory Evolution Restores Solvent Tolerance in Plasmid-
725 Cured *Pseudomonas putida* S12: a Molecular Analysis. *Appl Environ Microbiol* 87:1–18.
- 726 54. Ramos JL, Duque E, Gallegos M-T, Godoy P, Ramos-González MI, Rojas A, Terán W, Segura A.

- 727 2002. Mechanisms of Solvent Tolerance in Gram-Negative Bacteria. *Annu Rev Microbiol* 56:743–
728 768.
- 729 55. Mills TY, Sandoval NR, Gill RT. 2009. Cellulosic hydrolysate toxicity and tolerance mechanisms in
730 *Escherichia coli*. *Biotechnol Biofuels* 2:26.
- 731 56. Borges A, Ferreira C, Saavedra MJ, Simões M. 2013. Antibacterial Activity and Mode of Action of
732 Ferulic and Gallic Acids Against Pathogenic Bacteria. *Microb Drug Resist* 19:256–265.
- 733 57. Luke NR, Sauberan SL, Russo TA, Beanan JM, Olson R, Loehfelm TW, Cox AD, St. Michael F,
734 Vinogradov E V., Campagnari AA. 2010. Identification and Characterization of a
735 Glycosyltransferase Involved in *Acinetobacter baumannii* Lipopolysaccharide Core Biosynthesis.
736 *Infect Immun* 78:2017–2023.
- 737 58. Zhang G, Baidin V, Pahil KS, Moison E, Tomasek D, Ramadoss NS, Chatterjee AK, McNamara CW,
738 Young TS, Schultz PG, Meredith TC, Kahne D. 2018. Cell-based screen for discovering
739 lipopolysaccharide biogenesis inhibitors. *Proc Natl Acad Sci* 115:6834–6839.
- 740 59. May KL, Grabowicz M. 2018. The bacterial outer membrane is an evolving antibiotic barrier. *Proc*
741 *Natl Acad Sci* 115:8852–8854.
- 742 60. Cuff LE, Elliott KT, Seaton SC, Ishaq MK, Laniohan NS, Karls AC, Neidle EL. 2012. Analysis of
743 is1236-mediated gene amplification events in *Acinetobacter baylyi* ADP1. *J Bacteriol*.
- 744 61. Renda BA, Dasgupta A, Leon D, Barrick JE. 2015. Genome instability mediates the loss of key
745 traits by *Acinetobacter baylyi* ADP1 during laboratory evolution. *J Bacteriol*.
- 746 62. Kearse M, Moir R, Wilson A, Stones-Havas S, Cheung M, Sturrock S, Buxton S, Cooper A,
747 Markowitz S, Duran C, Thierer T, Ashton B, Meintjes P, Drummond A. 2012. Geneious Basic: An
748 integrated and extendable desktop software platform for the organization and analysis of

749 sequence data. Bioinformatics.

750 63. Deatherage DE, Barrick JE. 2014. Identification of Mutations in Laboratory-Evolved Microbes

751 from Next-Generation Sequencing Data Using breseq, p. 165–188. *In* .

752

753 **Tables and figure legends**

754 **Table 1.** Mutations in the evolved isolates.

Gene locus ID (name) ^a	Position ^a	Description ^a	Mutation type	DNA change	Protein effect	ASA 500	ASA 501	ASA 502	ASA 503
<i>ACIAD1702</i> (<i>pcaU</i>)	1708197	Regulatory protein for <i>pca</i> operon (activator)	Substitution (transition)	G → A	P250L (CCA→CTA)	+	+		
<i>ACIAD1722</i> (<i>hcaE</i>)	1730279-1730280	Porin	Insertion (tandem repeat)	(G)3 → (G)4	Frameshift			+	+
<i>ACIAD1722</i> (<i>hcaE</i>)	1730384-1730385	Porin	Insertion (IS element)	+IS, +AGG	Frameshift	+	+		
<i>ACIAD1727</i> (<i>hcaK</i>)	1736544-1736548 or 1736548-1736552	Transporter	Deletion	-TGCTG or -GTGCT	Frameshift*		+		
<i>ACIAD0982</i> (<i>vanK</i>)	967651-968787	Transporter	Deletion (> 1kb)	1137 bp deletion	Loss of function	+			
<i>ACIAD2867</i>	2807553	Putative Na ⁺ /H ⁺ antiporter	Substitution (transition)	G → A	A247V (GCA→GTA)	+			
<i>ACIAD2265</i>	2236575-2236576	Putative rare lipoprotein A family	Insertion	+C	Frameshift		+		
<i>ACIAD2365</i> (<i>msbA</i>)	2322575	Lipid transport protein	Substitution (transition)	G → A	A486V (GCG→GTG)			+	+
<i>ACIAD0648</i> (<i>secA</i>)	639202	Preprotein translocase	Substitution (transition)	C → T	P796L (CCA→CTA)			+	
<i>ACIAD0482</i>	476258-476269 or 476264-476275	putative glycosyltransferase	Deletion	-TGAGGAAAGGCT or -AAGGCTTGAGGA	Δ166-169	+			
<i>ACIAD0602</i>	591935	Putative glycosyltransferase	Deletion (tandem repeat)	(T)5 → (T)4	Frameshift			+	+
<i>ACIAD1405</i> (<i>iscR</i>)	1399615	Repressor of the <i>iscRSUA</i> operon	Substitution (transition)	G → A	Truncation			+	+
<i>ACIAD0260</i> (<i>gacA</i>)	261189	Response regulator	Deletion	-A	Frameshift			+	+
<i>ACIAD3465</i>	3392835	Putative two-component sensor	Substitution (transversion)	G → T	G881C (GGT→TGT)		+		
<i>ACIAD2274</i> (<i>sthA</i>)	2243241	Soluble pyridine nucleotide transhydrogenase	Substitution (transition)	G → A	A462V (GCT→GTT)			+	+
<i>ACIAD0438</i> (<i>rne</i>)	436298	Ribonuclease E	Deletion	-A	Frameshift		+		
<i>ACIAD3194</i> (<i>rpoA</i>)	3122059	RNA polymerase alpha subunit	Substitution (transversion)	G → T	P291Q (CCA→CAA)		+		
<i>ACIAD0308</i> (<i>rpoC</i>)	307439	RNA polymerase beta subunit	Substitution (transition)	A → G	D285G (GAT→GGT)			+	
<i>ACIAD1220</i>	1223930	Conserved hypothetical protein	Substitution (transversion)	C → G	G84A (GGA→GCA)	+			
<i>ACIAD3457</i> to <i>ACIAD3481</i>	3380313-3408297	N/A	Duplication (IS involved)	Duplication	N/A	+			
<i>ACIAD3459</i> to <i>ACIAD3486</i>	3380938-3413938	N/A	Duplication (IS involved)	Duplication	N/A				+
N/A	2808313-2808314	Non-coding region 21 bp upstream of <i>ACIAD2867</i>	Insertion (IS element)	+IS, +AAC	N/A			+	+
N/A	474157-474158	Non-coding region 135 bp upstream of <i>ACIAD0481</i>	Insertion (IS element)	+IS, +TGT	N/A			+	+
N/A	2766926-2766927	Non-coding region between <i>ACIAD2829</i> and <i>ACIAD2832</i>	Insertion (tandem repeat)	(T)6 → (T)7	N/A	+		+	+
N/A	2236147	Non-coding region between <i>ACIAD2264</i> (<i>mltB</i>) and <i>ACIAD2265</i>	Deletion (tandem repeat)	(T)7 → (T)6	N/A			+	+
N/A	967592	Non-coding region 17 bp upstream of <i>ACIAD0980</i> (<i>vanA</i>)	Substitution (transition)	C → T	N/A				+

755 * For HcaK, the UniProt entry Q7X0E0 (with 410 residues) was used as a reference to evaluate
756 the protein effect.

757 ^a Locus IDs, mutation positions, and descriptions were assigned according to the reference
758 genome CR543861 (GeneBank entry).

759 **Table 2.** Bacterial strains used in the study

Name	Description	Source / reference
<i>E. coli</i> XL1-Blue	Wild-type <i>E. coli</i> XL1-Blue	Stratagene, USA
WT ADP1	Wild-type <i>A. baylyi</i> ADP1	DSM 24193, DSMZ
ASA500	isolate from G1 evolution line	(23)
ASA501	isolate from G2 evolution line	(23)
ASA502	isolate from T2 evolution line	this study
ASA503	isolate from T2 evolution line	this study
ISx	Transposon-free <i>A. baylyi</i> ADP1	(42)
ASA504	reconstructed mutant containing <i>hcaE500</i> , descended from ISx, constructed by RAMSES with ferulate	this study
ASA505	reconstructed mutant containing <i>vanK500</i> , descended from ISx, constructed by RAMSES with ferulate	this study
ASA506	reconstructed mutant containing <i>hcaE500</i> and <i>vanK500</i> , descended from ASA504, constructed by RAMSES with vanillate	this study
ASA507	reconstructed mutant containing <i>hcaE500</i> and <i>hcaK501</i> , descended from ASA504, constructed by RAMSES with ferulate	this study
ASA508	reconstructed mutant containing <i>hcaE500</i> and <i>ACIAD0482_500</i> , descended from ASA504, constructed by RAMSES with ferulate	this study
ASA509	$\Delta vanKP::spec^r$ mutant descended from ASA504, 732 bp region upstream of <i>vanK</i> was also deleted	this study
ASA510	$\Delta vanP::spec^r$ mutant descended from ASA504	this study

760

761

762 **Table 3.** Primers used in the study

Name	Sequence	Description
pcaU-M-F	CATCAGGGCTGACTGCTGAA	forward primer used to amplify <i>pcaU500</i>
pcaU-M-R	CAATTTTGCCCGCACGGTAT	reverse primer used to amplify <i>pcaU500</i>
hcaE-M-F	GCCTTTGAGCTGAGCACCTA	forward primer used to amplify <i>hcaE500</i>
hcaE-M-R	AGTAACTCAGCGCCTTGGTC	reverse primer used to amplify <i>hcaE500</i>
hcaK-M-F	AAATCCATGCCAGCAGTCCA	forward primer used to amplify <i>hcaK501</i>
hcaK-M-R	ACGGCATTGATTTTGCCCA	reverse primer used to amplify <i>hcaK501</i>
vanK-M-F	TTCCACGTAACGCCATTTGC	forward primer used to amplify <i>vanK500</i>
vanK-M-R	GATATGCGCCACCCAAGGTA	reverse primer used to amplify <i>vanK500</i>
ACIAD2867-M-F	AGTTTGCTGAGTTGCCAGT	forward primer used to amplify <i>ACIAD2867_500</i>
ACIAD2867-M-R	GGCGTTCTGAACAATGCGAG	reverse primer used to amplify <i>ACIAD2867_500</i>
ACIAD2265-M-F	TGGCAACGTAACCAACCAGT	forward primer used to amplify <i>ACIAD2265_501</i>
ACIAD2265-M-R	ACATTGCTACAGCCAGCACT	reverse primer used to amplify <i>ACIAD2265_501</i>
ACIAD0482-M-F	TGGTCTTGGTTTACGCAGCA	forward primer used to amplify <i>ACIAD0482_500</i>
ACIAD0482-M-R	TCGTTGCCGTGCAACTATCT	reverse primer used to amplify <i>ACIAD0482_500</i>
P1-F	ATGGTACCCACACTGGATATGAAAC AGC	forward primer used to amplify the left flanking sequence for <i>vanKP</i> knock-out, contains KpnI site
P2-R	ATACTCGAGATTAATAAAATAGGA TTGACTCTGC	reverse primer used to amplify the left flanking sequence for <i>vanKP</i> knock-out, contains XhoI site
P3-F	TATCCTAGGTCATTCAACCAACGAA ACACG	forward primer used to amplify the right flanking sequence for <i>vanKP</i> and <i>vanP</i> knock-out, contains AvrII site
P4-R	ATTACGAATTCTTCATCCAAAACGCA AAAGCC	reverse primer used to amplify the right flanking sequence for <i>vanKP</i> and <i>vanP</i> knock-out, contains EcoRI site
P5-F	TAGGTACCGCTGGACACCAAAAATT CTGA	forward primer used to amplify the left flanking sequence for <i>vanP</i> knock-out, contains KpnI site
P6-R	ATACTCGAGTTAAGCAACTGTTTTT ATAGAACTTC	reverse primer used to amplify the left flanking sequence for <i>vanP</i> knock-out, contains XhoI site
spec-F	GTCAATCCTATTTTATTTAATCTCGA GTATGCAGAAAGGAGAAGCTTACTA G	forward primer used to amplify the spectinomycin resistance gene, contains XhoI site
spec-R	CGTTGGTTGAATGACCTAGGATAGC TTAATGCGCCGCTACA	reverse primer used to amplify the spectinomycin resistance gene, contains AvrII site

763 **Figure 1.** Growth of ASA500, ASA501, and WT ADP1 on ferulate, vanillate, and *p*-coumarate.
764 (A) Possible transport system (porins colored in green and transporters colored in blue) for
765 aromatic acids and the β -ketoadipate pathway in ADP1. The pathway indicated by the dashed
766 arrow involves multiple steps. (B) Growth of the strains ASA500, ASA501, and WT ADP1 at
767 different concentrations of ferulate, vanillate, and *p*-coumarate. All the strains were cultivated in
768 mineral salts media with the corresponding aromatic compound as the sole carbon source. The
769 time needed for the cells to reach the OD of 0.8 was used as the indicator to evaluate the tolerance
770 ($t_{OD\ 0.8}$). The indicator is calculated only when both replicates reached OD 0.8 within 48 h. Grey
771 horizontal lines indicate the 0.8 OD threshold. All the values were calculated from two replicates
772 and the error bars indicate the standard deviations. The y-axis is shown in log₁₀ scale.

773 **Figure 2.** Number of mutations in the genomes of each evolved strain.

774 **Figure 3.** Temporal occurrence of the mutations in *hcaE* and *vanK* in G1 and G2 evolution
775 populations. (A) The *hcaE* mutation caused by IS1236 insertion and gel electrophoresis showing
776 the genotypic change in *hcaE* in G1 and G2 evolution populations sampled on different days. (B)
777 Deletion in the *vanK* region and the genotypic change of this region in G1 evolution populations
778 over time. The deletion of 1137 bp (highlighted in blue) extends from the upstream of *vanK* to its
779 CDS position of nucleotide 405.

780 **Figure 4.** Schematic of RAMSES. The mutated allele amplified from the evolved strain is used to
781 transform the background strain by direct addition of the purified PCR product to the exponentially
782 growing cells (in small volume) or newly emerging colony. The linear DNA is incorporated into
783 the chromosome by allelic replacement. The cultures after transformation are used to inoculate
784 different media with incremental selective pressures (here aromatic concentration) in a multi-well
785 plate. The growth is monitored based on the measurement of optical density. The mutants (colored

786 in red) containing the advantageous mutation can grow robustly and get enriched at the level of
787 selective pressure such that it outcompetes the background strain, resulting in a different growth
788 profile compared to the control. The mutant can be recovered from the culture by an additional
789 enrichment step under the same (or higher) selective pressure and subsequent isolation, and the
790 corresponding mutation(s) can be confirmed by sequencing (or PCR if possible).

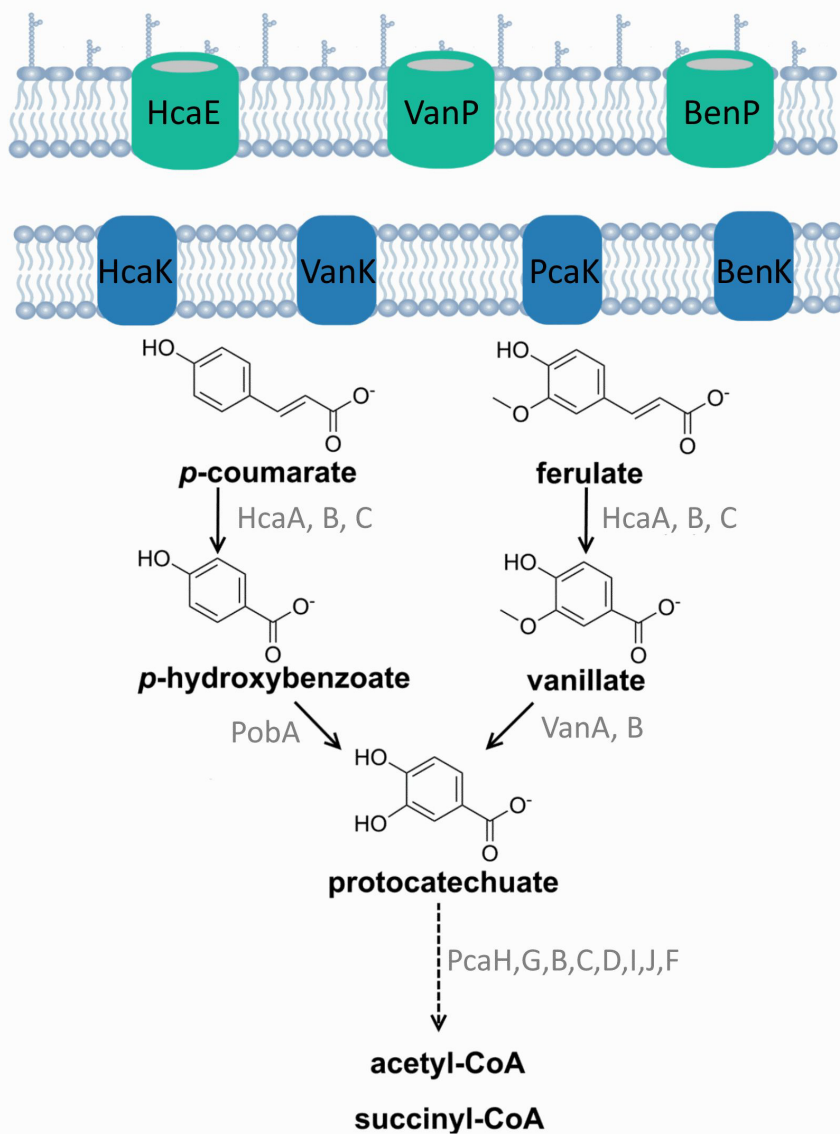
791 **Figure 5.** Initial screening of advantageous mutations by RAMSES. Growth of ISx in 60 mM
792 ferulate after being transformed with the selected mutated alleles is shown. Control 1: ISx without
793 any treatment. Control 2: ISx treated with water. Control 3: ISx treated with a non-mutated allele.
794 The OD values were calculated from two replicates. The error bars indicate the standard deviations.
795 The y-axis is shown in log₁₀ scale.

796 **Figure 6.** Reverse engineering of the selected mutations by RAMSES. (A) Reverse engineering
797 of *hcaE500* into ISx. Growth of ISx in 20 mM ferulate after transformation is shown. Control: ISx
798 without transformation. To analyze *hcaE*, PCR analysis was performed from the genome of the
799 transformed population after further enrichment. Lane 1: the transformed population. (B) Reverse
800 engineering of *vanK500* into ASA504 (reconstructed mutant *hcaE*). Growth of ASA504 in 40 mM
801 vanillate after transformation is shown. Control: ASA504 without transformation. To analyze
802 *vanK*, PCR analysis was performed from the genome of the transformed population after further
803 enrichment. Lane 1: the transformed population. Lane 2: ASA504 containing wild-type *vanK*. (C)
804 Reverse engineering of *hcaK501* and *ACIAD0482_500* into ASA504 (reconstructed mutant *hcaE*).
805 Growth of ASA504 in 60 mM ferulate after transformation is shown. Control: ASA504 without
806 transformation. The genes *hcaK* and *ACIAD0482* of the single isolates from the enriched
807 populations were analyzed by sequencing. Pure mutant strains were recovered by further isolation.

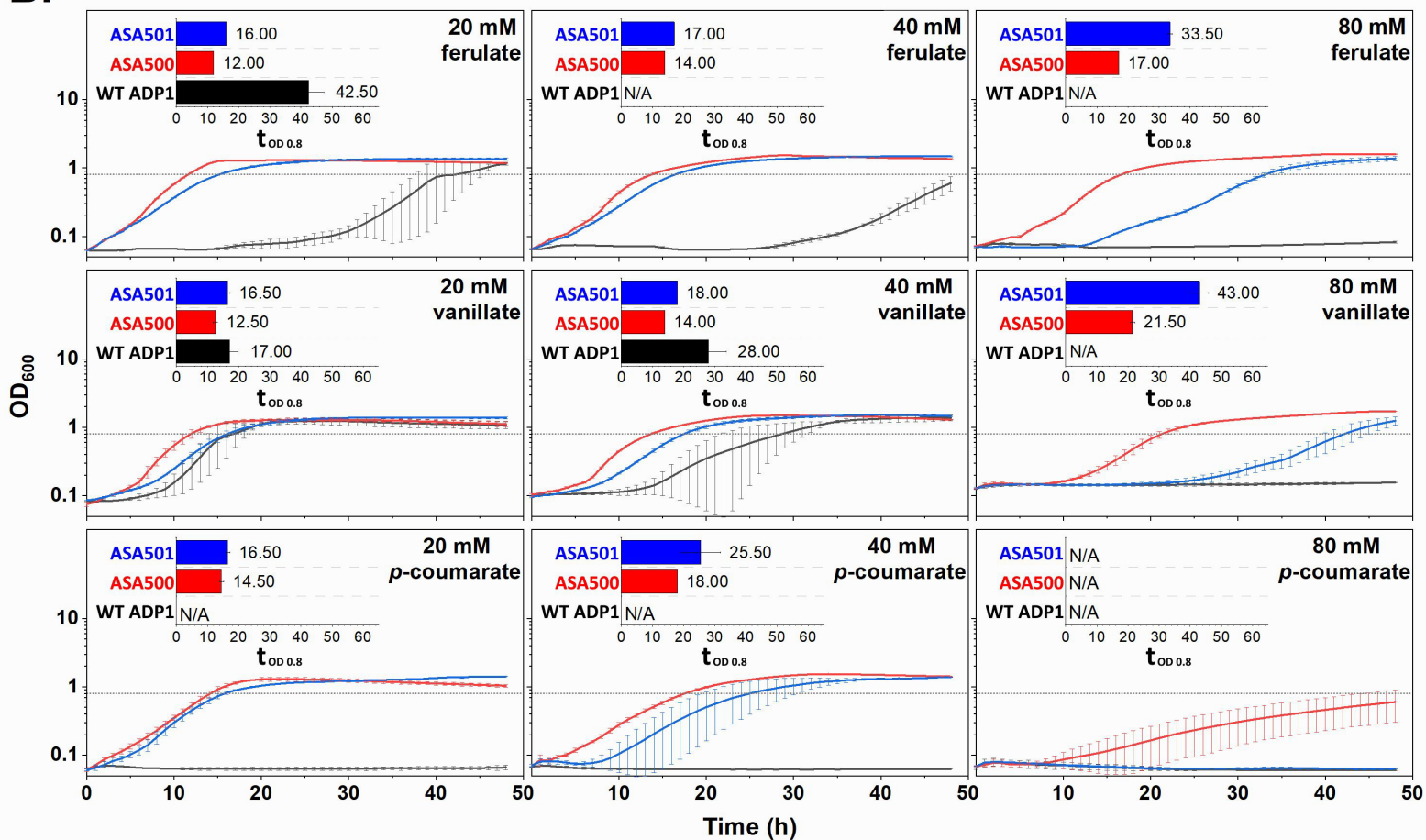
808 (D) The reconstructed strains derived from ISx. The OD values were calculated from two replicates.
809 The error bars indicate the standard deviations. The y-axis is shown in log₁₀ scale.

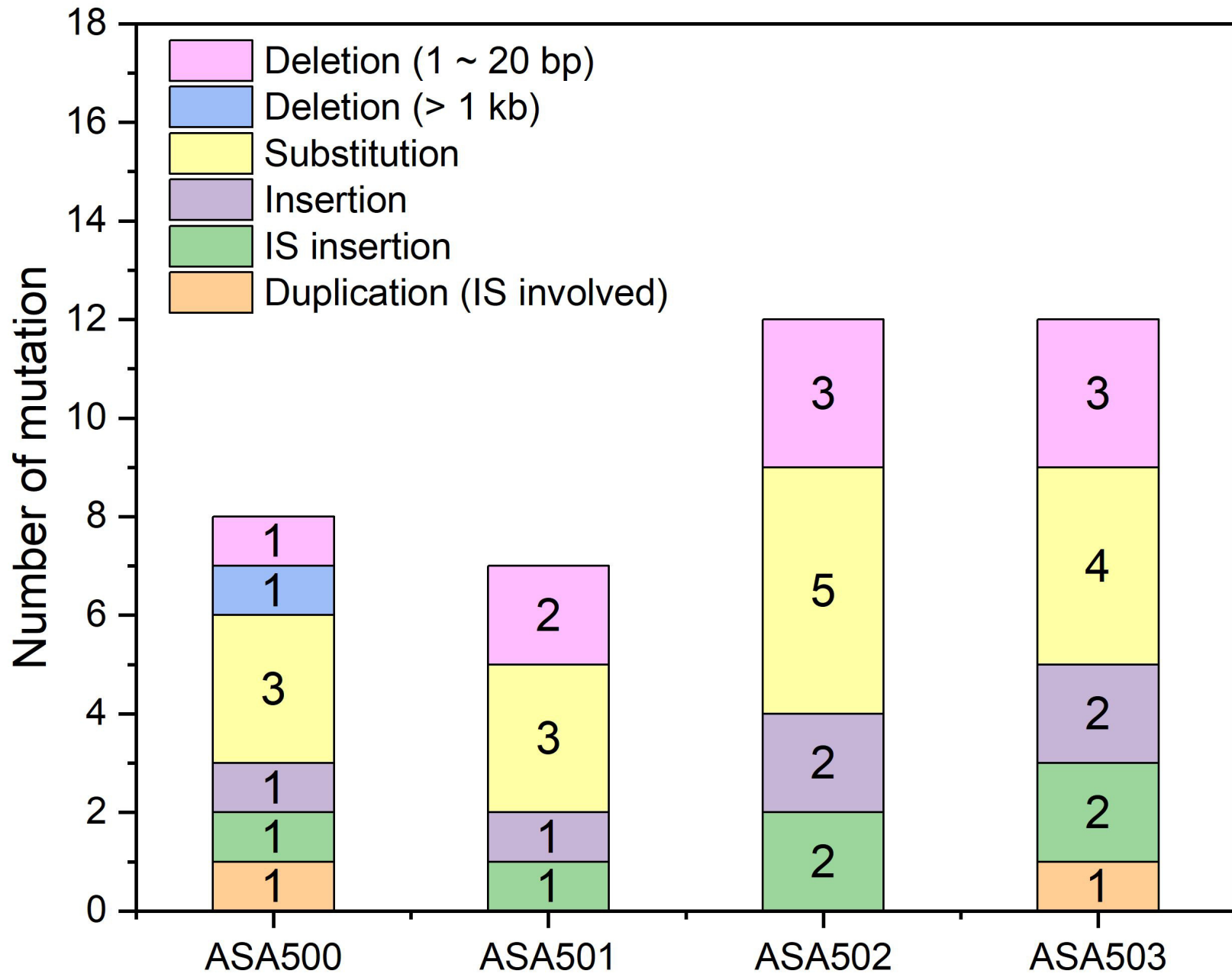
810 **Figure 7.** Growth comparison between the reconstructed strains at different ferulate concentrations
811 (20 mM, 40 mM, and 60 mM). ASA500 and ASA 501 are the evolved strains, and ASA504-508
812 are the reconstructed strains. All the strains were cultivated in mineral salts media with the ferulate
813 as the sole carbon source. The time needed for the cells to reach the OD of 0.8 was used as the
814 indicator to evaluate the tolerance ($t_{OD\ 0.8}$). The indicator was calculated only when both replicates
815 reached OD 0.8 within 48 h. Grey horizontal lines indicate the 0.8 OD threshold. All the values
816 were calculated from two replicates and the error bars indicate the standard deviations. The y-axis
817 is shown in log₁₀ scale.

A.

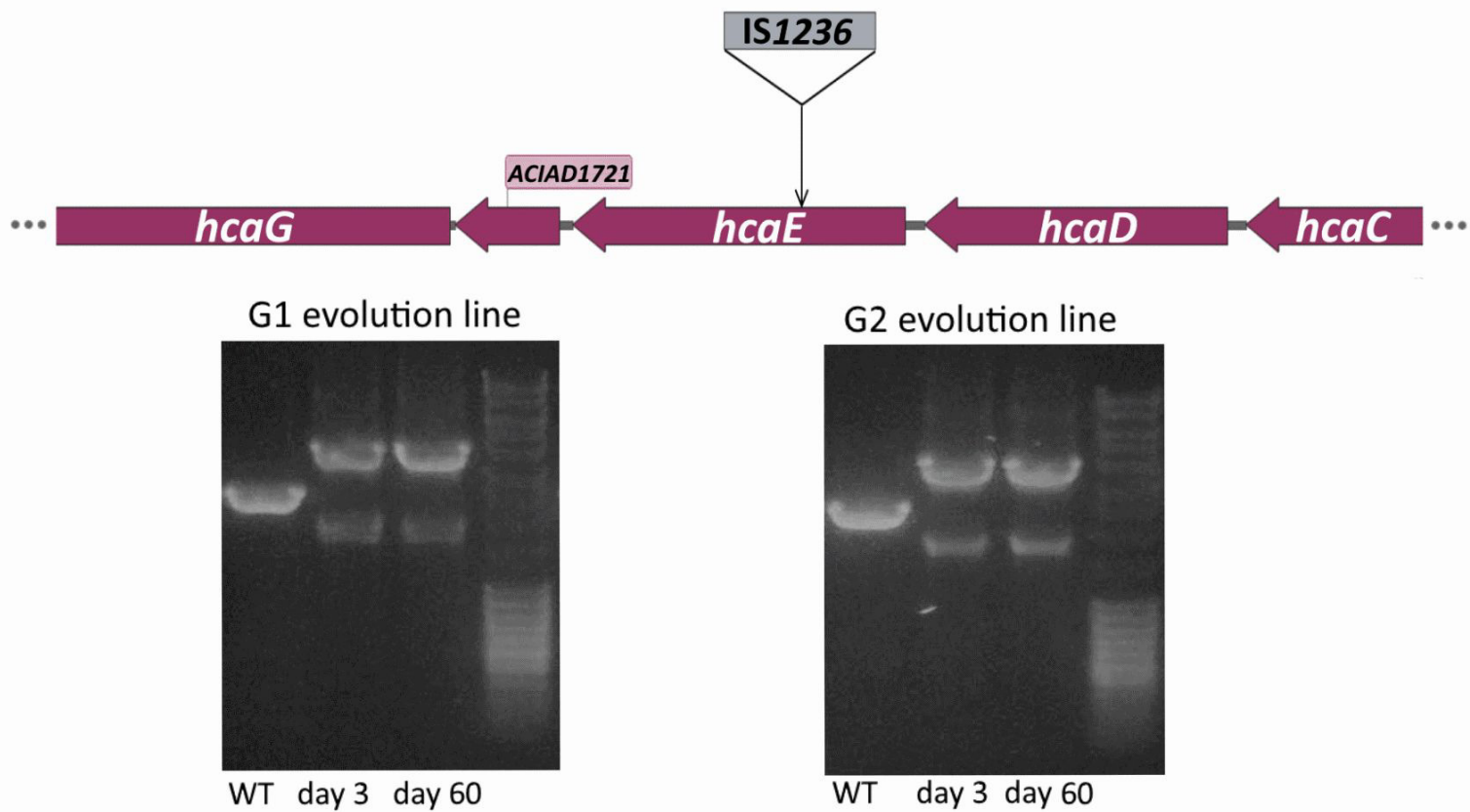


B.

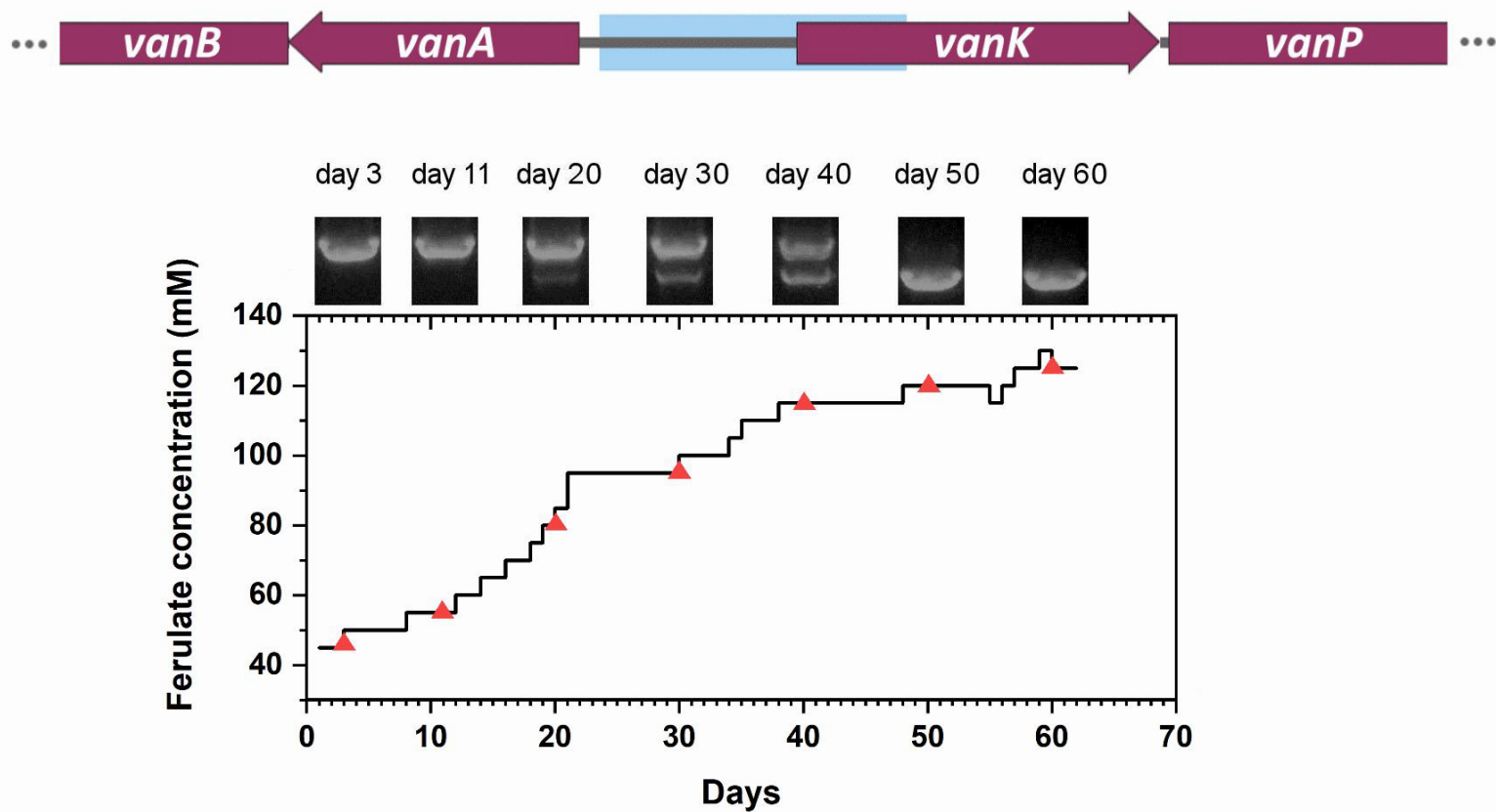




A.

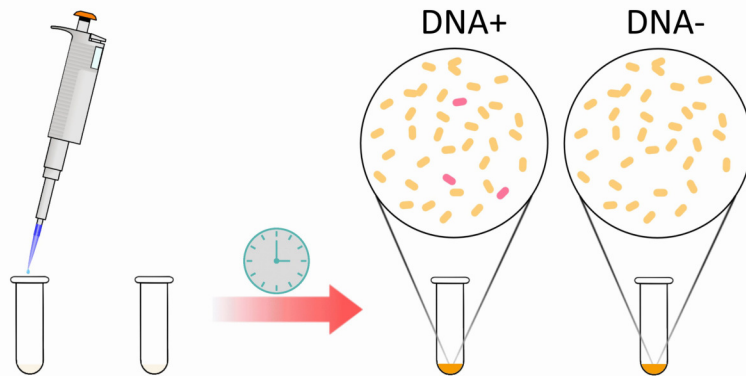


B.



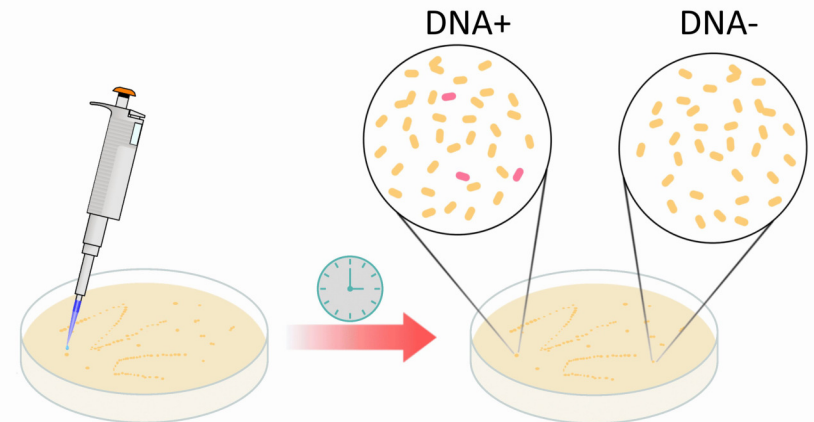
Liquid medium transformation

- Addition of the amplified mutated allele to the cell culture (DNA+)
- The culture without DNA addition as a control (DNA-)



Solid medium transformation

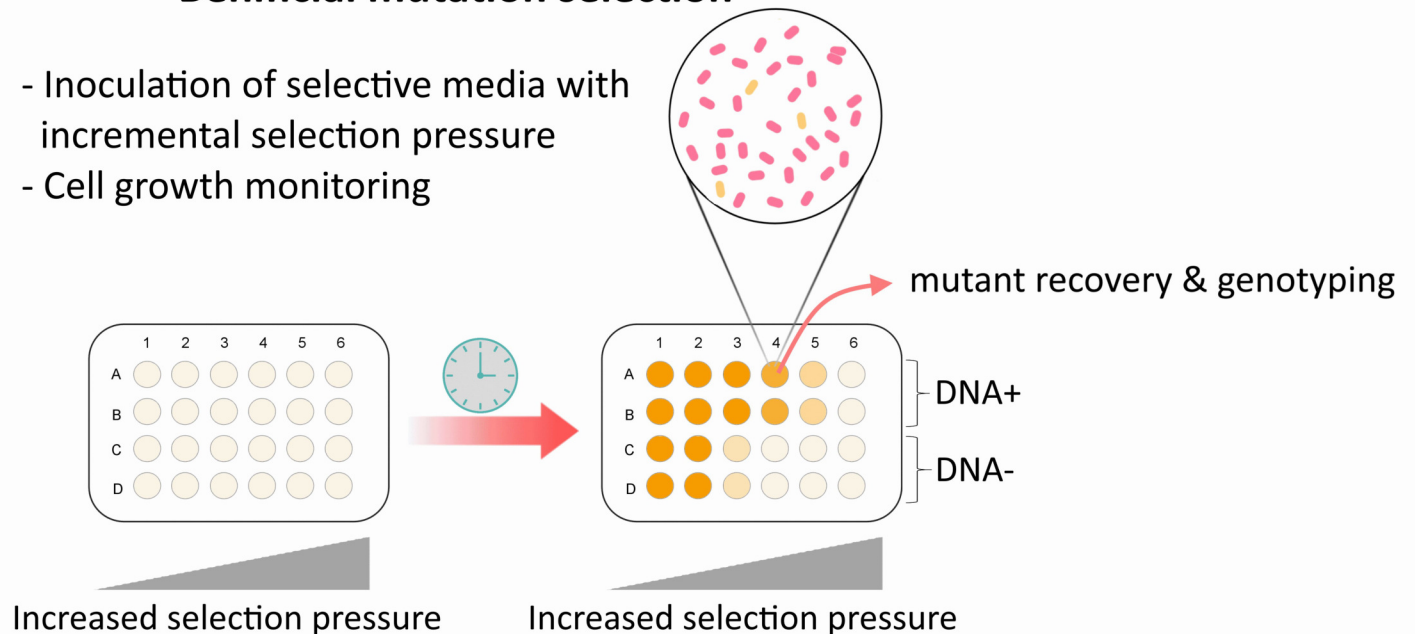
- Addition of the amplified mutated allele to a single colony (DNA+)
- A colony without DNA addition as a control (DNA-)

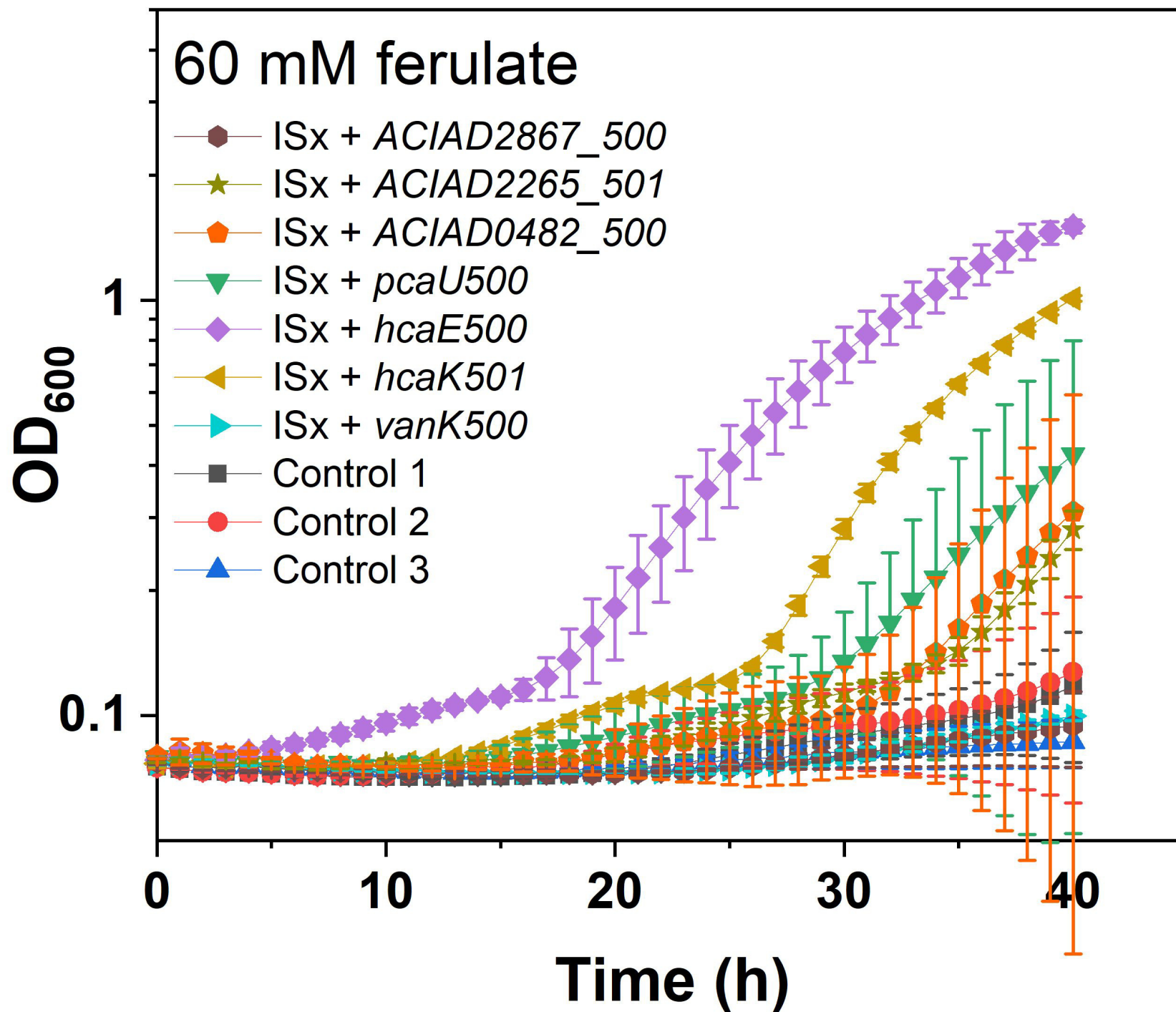


or

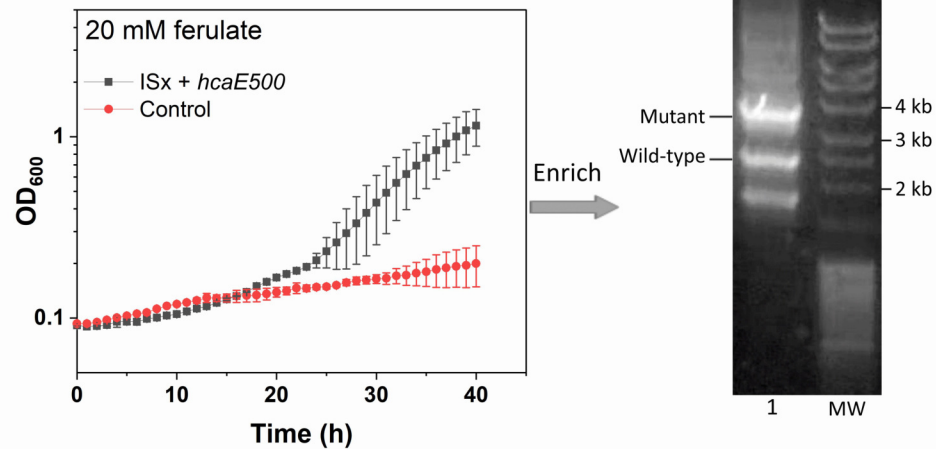
Beneficial mutation selection

- Inoculation of selective media with incremental selection pressure
- Cell growth monitoring

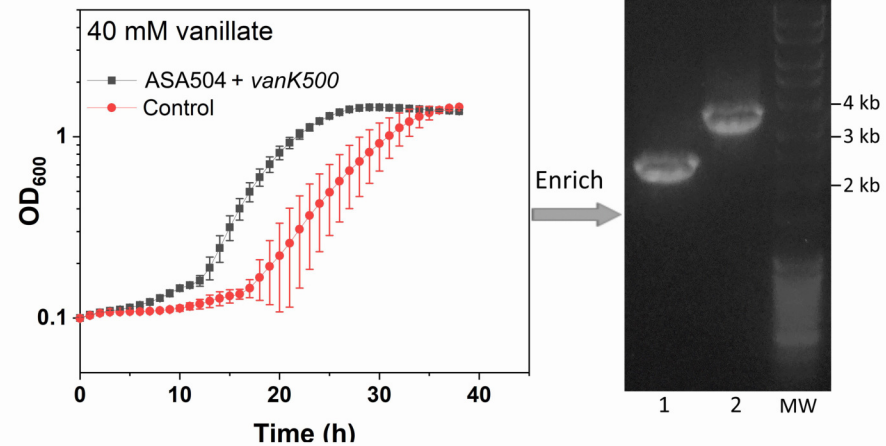




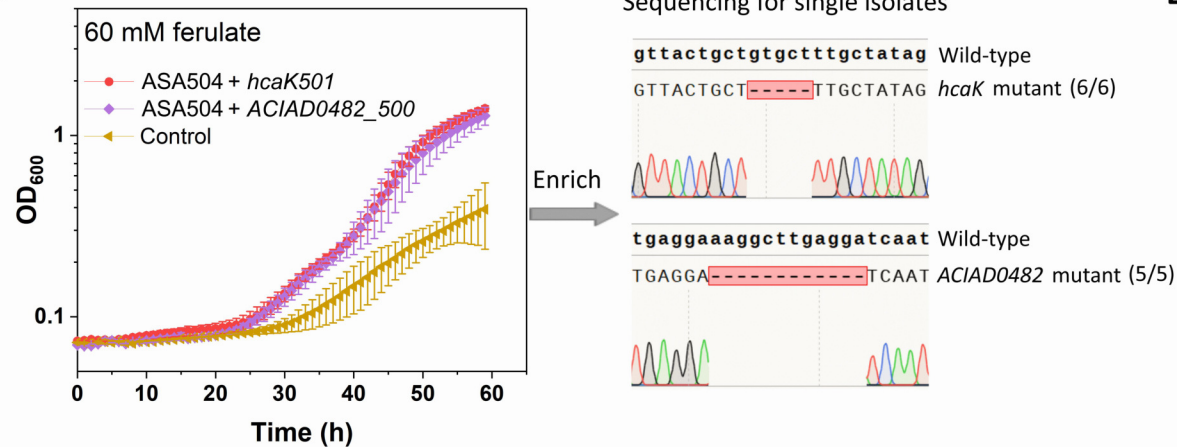
A.



B.



C.



D.

